Tectonic evolution of a Paleozoic thrust fault influences the hydrogeology of a fractured rock aquifer, northeastern Appalachian foreland

J. Kim, P. Ryan, K. Klepeis, T. Gleeson, K. North, J. Bean, L. Davis, J. Filoon

August 2014

http://dx.doi.org/10.1111/gfl.12076

GEOFLUIDS

Geofluids (2014) **14**, 266–290 doi: 10.1111/gfl.12076

Tectonic evolution of a Paleozoic thrust fault influences the hydrogeology of a fractured rock aquifer, northeastern Appalachian foreland

J. KIM[1], P. RYAN[2], K. KLEPEIS[3], T. GLEESON[4], K. NORTH[2], J. BEAN[2], L. DAVIS[2] AND J. FILOON[2]

[1]*Vermont Geological Survey, Montpelier, VT, USA;* [2]*Department of Geology, Middlebury College, Middlebury, VT, USA;* [3]*Department of Geology, University of Vermont, Burlington, VT, USA;* [4]*Department of Civil Engineering, McGill University, Montréal, QC, Canada*

ABSTRACT

In polyorogenic regions, the superposition of structures during a protracted tectonic history produces complex fractured bedrock aquifers. Thrust-faulted regions, in particular, have complicated permeability patterns that affect groundwater flow paths, quantity, and quality. In the Appalachian foreland of northwestern Vermont, numerous bedrock wells that are spatially related to the Paleozoic Hinesburg thrust have elevated naturally occurring radioactivity and/or low yields. The association of groundwater quality and quantity issues with this thrust was a unique opportunity to investigate its structural and hydrogeologic framework. The Hinesburg thrust juxtaposed metamorphic rocks of the hanging wall with sedimentary rocks of the footwall during the Ordovician. It was then deformed by two orthogonal Devonian fold sets and was fractured during the Cretaceous. Median well yields in the hanging wall aquifer are significantly lower than those of the footwall aquifer, consistent with the respective permeability contrast between metamorphic and carbonate rocks. For wells drilled through the Hinesburg thrust, those completed closest (vertically) to the thrust have the highest median yields, whereas others completed farther below have yields in the footwall range. The geochemical signature of the hanging wall and footwall aquifers correlates with their whole-rock geochemistry. The hanging wall aquifer is enriched in alpha radiation, Na+K-Cl, Ba, and Sr, whereas the footwall aquifer is enriched in Ca-Mg-HCO_3 and alkalinity. Wells that penetrated the Hinesburg thrust generally have hanging wall geochemical signatures. A simple hydrogeologic model for the permeability evolution of the Hinesburg thrust involves the ductile emplacement of a low-K hanging wall onto a high-K footwall, with subsequent modification by fractures.

Key words: Appalachians, foreland, fractured rock aquifer, groundwater chemistry, hydrogeology, naturally-occurring radioactivity, tectonic evolution, thrust fault

Received 12 July 2013; accepted 10 January 2014

Corresponding author: Jonathan Kim, Vermont Geological Survey, One National Life Dr., Davis 2, Montpelier, VT 05620-3902, USA.
Email: jon.kim@state.vt.us. Tel: 802/522-5401. Fax: 802-828-1250.

Geofluids (2014) **14**, 266–290

INTRODUCTION

Fractured bedrock aquifers are important groundwater resources in many parts of the world. The hydrogeologic framework of these aquifers is often dominated by anisotropic polydeformed metamorphic rocks where ductile and brittle structures are superposed during a protracted tectonic history (e.g., Gunderson 1991; Seaton & Burbey 2005). In particular, faulted bedrock aquifer systems have complicated permeability patterns that affect groundwater flow paths, quantity, and quality (e.g., Caine *et al.* 2010; Bense *et al.* 2013).

In northwestern Vermont, elevated naturally occurring radioactivity (alpha radiation, uranium, and radium) was discovered in groundwater from a bedrock public water supply well (Bazilchuk 2000; Kim & Becker 2001, 2004) and subsequently in numerous private wells drilled into the hanging wall of the Paleozoic Hinesburg thrust fault (Fig. 1). In addition to elevated radioactivity, some proposed housing developments in the same region were

abandoned due to insufficient groundwater quantity, and an increasing number of domestic wells are now being drilled through the Hinesburg thrust into more productive sedimentary rocks of the footwall to meet domestic groundwater demands.

Within fractured rock aquifers, thrust faults have complex permeability patterns that affect groundwater flow paths and consequently groundwater quantity and the distribution and transport of naturally occurring contaminants (e.g., Caine *et al.* 1996, 2010; Bense *et al.* 2013). The strong contrast in productivity between wells completed in the footwall versus hanging wall of the Hinesburg thrust also raises new questions about what controls groundwater flow and bedrock aquifer development in this region. Because of multiple generations of ductile and brittle deformation, polyorogenic areas such as the northwestern Vermont foreland are particularly challenging for understanding the physical and chemical controls on groundwater flow around fault zones. However, the coincidence of water quality and quantity problems in bedrock wells that are in close proximity (vertically or horizontally) to the Hinesburg thrust makes this area unique for evaluating the role that this fault plays in both issues. Over the past decade, we devised a multidisciplinary study that incorporates stratigraphy, structural geology, physical hydrogeology, and groundwater and whole-rock geochemistry (including chlorofluorocarbon ages) to approach these issues.

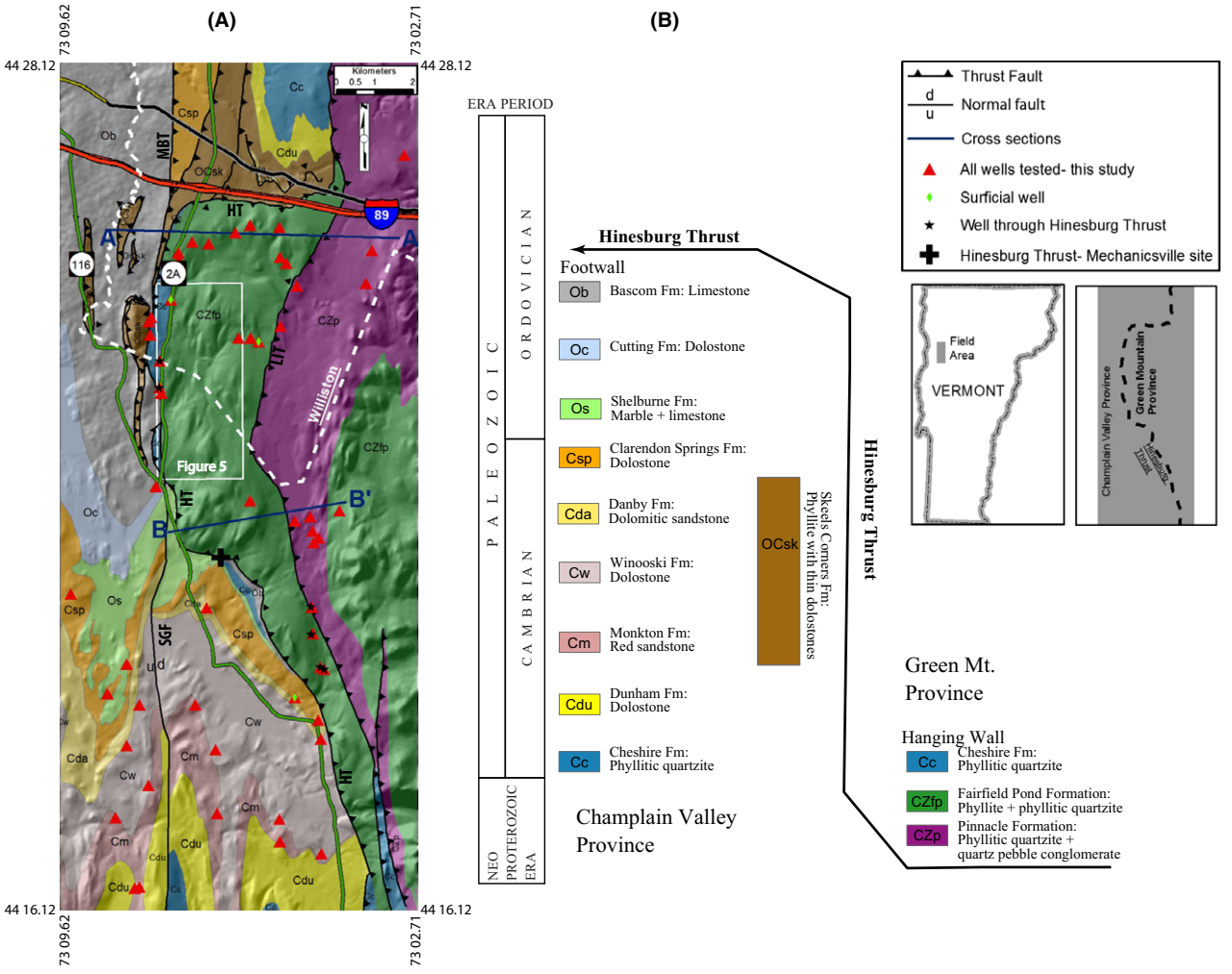

Fig. 1. (A) Bedrock geologic map for the field area that shows the locations of cross-sections, bedrock wells sampled for groundwater chemistry, and major roads. Compiled from Kim *et al.* (2007), Thompson *et al.* (2004), and Mehrtens (1997). HT = Hinesburg Thrust; MBT = Muddy Brook Thrust; SGF = St. George Fault; LIT = Lake Iroquois Thrust; 'd' and 'u' indicate down and up motions on normal fault; thrust faults have teeth on the upper plate; bold white dashed line shows the boundary of the Town of Williston in the field area; the location of Fig. 5 is also shown; shaded relief underlay displays the general topography; first inset map shows the location of the field area in Vermont, whereas the second shows the division of the field area into the Champlain Valley and Green Mountain geologic provinces; and (B) Simplified lithotectonic diagram for the field area that shows the major lithologies (and their ages) in the hanging wall and footwall of the Hinesburg thrust.

Using the previously mentioned disciplines, the objective of this paper is to document the protracted and complex structural evolution of the Hinesburg thrust from the Ordovician to the present and to assess the role that this progression played in the current physical and chemical hydrogeology of this thrust. We will highlight that the Hinesburg thrust formed at depth as a ductile fault (Ordovician), moved a second time after 'locking up', was subsequently deformed twice during the Devonian Acadian orogeny by orthogonal map-scale folds and lastly was pervasively fractured during Cretaceous extensional events. A relatively simple model is envisioned to integrate the hydrogeology and structural geology of the Hinesburg thrust, which involves the ductile emplacement of low-permeability metamorphic rocks of the hanging wall onto high-permeability sedimentary rocks of the footwall. The fault zone interface of mylonites on the hanging wall side and recrystallized and imbricated carbonates on the footwall side likely have the same permeabilities as their respective protoliths. This structural framework allows for a strong contrast in well yields and the downward infiltration of hanging-wall-derived groundwater. The permeability of the hanging wall and thrust zone was likely enhanced by fracture development, which may have been localized by previous episodes of cleavage development.

The building blocks of this study will now be presented in four separate sections entitled Stratigraphy and Tectonics, Structural Geology, Hydrogeology, and Aqueous and Bedrock Geochemistry. Each section is presented in considerable detail and then all are integrated together in the Discussion. The final section is an Epilog, which discusses how this hydrogeological information was used to inform environmental policy.

STRATIGRAPHY AND TECTONICS

In west central Vermont, the gently east-dipping, west-directed Hinesburg thrust is a major tectonic boundary between the Champlain Valley and Green Mountain Geologic provinces (Fig. 1). This thrust fault emplaced late Proterozoic to early Cambrian lower greenschist-facies metasedimentary (muscovite–biotite grade) and metaigneous rocks of the hanging wall/east side (Green Mountains) over weakly metamorphosed Lower Cambrian to Middle Ordovician carbonate and clastic sedimentary rocks of the footwall/west side (Champlain Valley), during the Ordovician Taconian orogeny (e.g., Gillespie 1975; Dorsey *et al.*, 1983; Stanley & Ratcliffe 1985; Stanley *et al.* 1987; Strehle & Stanley 1986; Kim *et al.* 2007, 2011). Other tectonic events to affect the field area include the Devonian Acadian orogeny and extension associated with Cretaceous magmatism (e.g., McHone 1978). Using simple line-balanced retro-deformation methods, Stanley *et al.* (1987), Stanley & Wright (1997) proposed that the Hinesburg thrust had a horizontal displacement of approximately 6 km.

The Pinnacle (CZp), Fairfield Pond (CZfp), and Cheshire (Cc) formations (Fig. 1) are the important lithologies in the hanging wall of the Hinesburg thrust. Both the Pinnacle and Fairfield Pond formations were deposited as clastic sediments in rift basins during Neoproterozoic rifting of the Rodinian supercontinent from approximately 590–554 Ma (e.g., Dorsey *et al.* 1983; Kumarpelli *et al.* 1989; Coish & Sinton 1992; Cherichetti *et al.* 1998; Walsh & Aleinikoff 1999). Continued rifting ultimately formed the Iapetus Ocean (e.g., van Staal *et al.* 1998) between the subcontinents of Laurentia and Gondwana. The Cheshire formation, which forms the base of the overlying passive continental margin sequence, was deposited upon the Fairfield Pond formation after the rift to drift transition. Because of structural repetition, the Cheshire formation is found both in the hanging wall and footwall of the Hinesburg thrust. Brief descriptions of the lithologic units and their general structural context in the hanging wall and field area are presented in Fig. 1.

The footwall of the Hinesburg thrust is dominantly comprised of carbonate and clastic sedimentary rocks, with the fault-bounded phyllites of the Skeels Corners formation being the exception. These rocks were deposited on the passive Laurentian continental margin as spreading in the Iapetus Ocean continued from the early Cambrian into the Middle Ordovician. The stratigraphy of these slices has been discussed in detail by Cady (1945), Welby (1961), Fisher (1968), Dorsey *et al.* (1983), Mehrtens & Dorsey (1987), Mehrtens & Hadley (1995), Mehrtens (1997), Mehrtens & Borre (1989), and Landing *et al.* (2003). The carbonate rocks of the Shelburne, Cutting, and Bascom formations (from oldest to youngest) are considered part of the Beekmantown Group whereas the older formations (oldest to youngest) Cheshire (quartzite), Dunham (dolostone), Monkton (quartzite), Winooski (dolostone), Danby (dolomitic sandstone), and Clarendon Springs (dolostone) are generally correlative with older members of the Potsdam Sandstone and Altona Formation of New York State (e.g., Fisher 1968; Landing *et al.* 2009).

STRUCTURAL GEOLOGY

Structures in the field area can be divided into three general age groupings (D_n = deformation event sequence), which include Ordovician (Taconian = D_1, D_2), Devonian (Acadian = D_3, D_4), and Cretaceous (D_5) events. Bedding in sedimentary rocks of the footwall is considered to be S_0. The relative structural chronology was determined through superposition and cross-cutting relationships. To display the structural complexity as simply as possible, a generalized three-dimensional diagram was constructed (Fig. 2) accompanied by Table 1, that describes the detailed

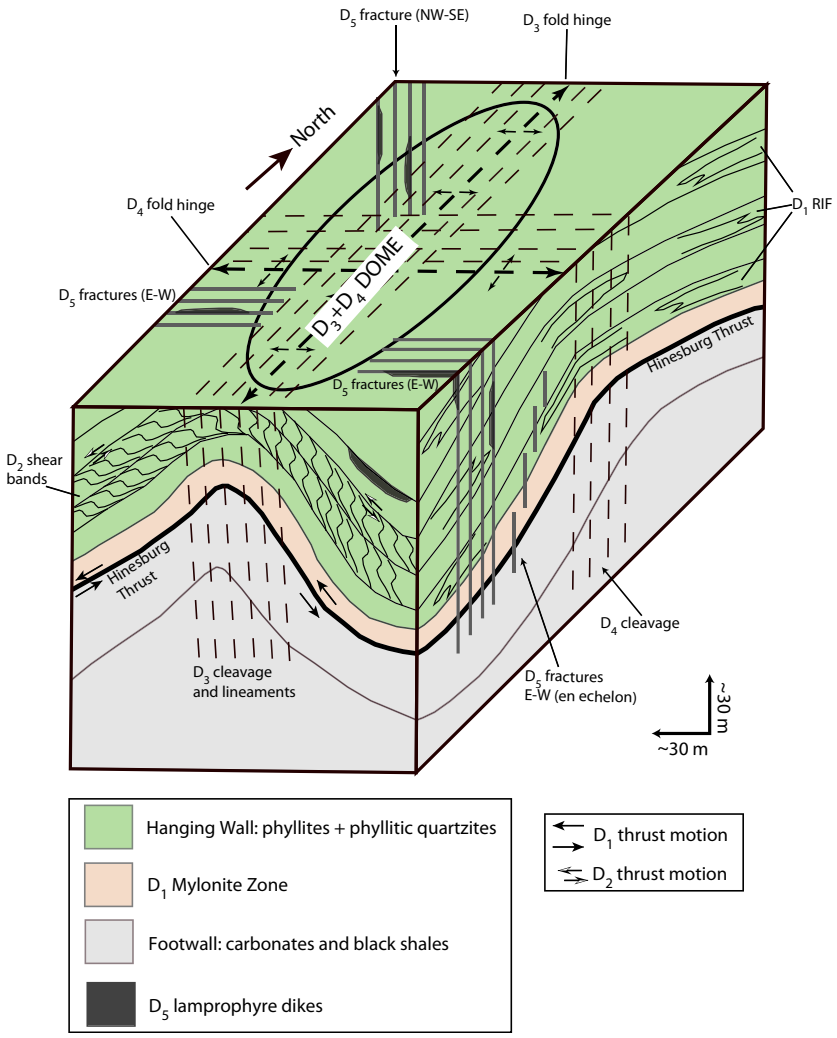

Fig. 2. Idealized structural model for the Hinesburg thrust that shows the five superposed deformational episodes (D_1–D_5), which span in age from the Ordovician to the Cretaceous. Although both domes and basins exist in the field area, this model is only drawn for a single dome. See text for details.

structures, their ages, and applicable references. Figure 2 provides a unifying framework for this section and the later hydrogeology and groundwater geochemistry sections.

The Hinesburg thrust is particularly well exposed at an extensive outcrop in the field area (at Mechanicsville) (see Fig. 1 for location) where overturned phyllitic quartzites of the Cheshire formation (hanging wall) structurally overlie dolostone slivers of the Bascom formation (footwall) (Fig. 3A). At this location, it is a ductile shear zone that is marked in the hanging wall by D_1 mylonites, ultramylonites, and phyllonites within a meter of the thrust contact (Fig. 3B). Rootless and reclined D_1 isoclinal folds are also prevalent that have stretching lineations collinear with their axes and the W-NW transport direction of the thrust (Fig. 3B); these folds are generally considered to be sheath folds. There are multiple generations of quartz veins in this fault zone, most of which are pre-syn D_1 (Strehle & Stanley 1986; Kim *et al.* 2011). As summarized by Passchier & Trouw (2005), mylonites are foliated and lineated rocks that were dominantly deformed by ductile flow; the grain size of these rocks was reduced from the protolith by recrystallization and intracrystalline deformation. The protolith of the Mechanicsville mylonites, based on comparisons with less deformed rocks of the Cheshire formation, was a shaly quartzite. The recrystallized mylonitic rocks contain primarily quartz and sericite, and the phyllonites are essentially mica-rich mylonites. Based on the intensity of fault-related fabrics in the hanging wall, Strehle & Stanley (1986) approximated the thickness of the thrust zone at 10–15 m. The dolostone in the footwall has multiple generations of quartz veins (Fig. 3D) and was deformed by the processes of fracturing, recrystallization, and pressure solution (Strehle & Stanley 1986) (Fig. 3D).

East of the Hinesburg thrust front, the D_1 foliation in the muscovite-biotite grade metamorphic rocks of the hanging wall, is a spaced cleavage in phyllitic quartzites that is characterized by alternating, parallel to anastomosing, quartz/feldspar and mica domains. In phyllitic units, the D_1 continuous cleavage is defined by aligned zones of abundant sericite and chlorite.

Table 1 Ductile and brittle structures that affected the hanging wall and footwall of the Hinesburg thrust in the field area with applicable references.

Generation	Period	Orogeny	Structure	Attitude planar + linear (general)	Citations
D_5	Cretaceous (approximately 120 Ma)		East–west trending fractures	Steep dips to north or south	Kim *et al.* (2007); Whitehead (2008); Gale *et al.* (2009)
			East–west trending en echelon fractures	Steep dips to north or south	Kim *et al.* (2011); Gale *et al.* (2012)
			NNE-trending fractures	Steep dips to east or west	
			NW-trending fractures	Steep dips to northeast or southwest	
			Lamprophyres	Intrude all fracture sets and foliations above	Armstrong & Stump (1971); McHone & Corneille 1980)
D_4	Devonian (approximately 390–380 Ma)	Acadian	F_4 open-tight asymmetric folds-axial surface	East–west trending, steep dip north or south	Kim *et al.* (2007); Kim *et al.* (2011); Gale *et al.* (2012)
			F_4 fold axis/crenulation lineation (L_4)	Shallow-moderate plunge east or west	
			S_4 crenulation or disjunctive cleavage	East–west trending, steep dip north or south	
D_3	Devonian (approximately 390–380 Ma)	Acadian	F_3 open-tight asymmetric folds-axial surface	NNE-trending steeply east-dipping	Strehle & Stanley (1986); Kim *et al.* (2011); West *et al.* (2011)
			F_3 fold axis/crenulation lineation (L_3)	Shallow plunge north or south	Dorsey *et al.* (1983); Kim *et al.* (2007); Gale *et al.* (2012)
			S_3 crenulation or disjunctive cleavage	NNE-trending steeply east-dipping	Tauvers (1982); DiPietro (1983)
D_2	Ordovician (approximately 460–450 Ma)	Taconian	F_2 asymmetric shear bands	NNE-striking, east-dipping	Strehle & Stanley (1986); Kim *et al.* (2011)
			L_2 intersection lineation (S_1 on S_2)	Down-dip plunge to east	
D_1	Ordovician (approximately 460–450 Ma)	Taconian	Hinesburg thrust and mylonites	NNE-striking, east-dipping	Gillespie (1975); Strehle & Stanley (1986); Thompson *et al.* (2004); Kim *et al.* (2011); West *et al.* (2011)
			F_1 reclined isoclinal folds-axial surface	NNE-striking, east-dipping	Dorsey *et al.* (1983); Kim *et al.* (2007); Gale *et al.* (2012)
			S_1 spaced foliation	NNE-striking, east-dipping	Tauvers (1982); DiPietro (1983)
			F_1 reclined isoclinal folds – fold axis/stretching lineation (L_1)	Down-dip plunge to east	

The D_2 top-to-the-west asymmetric shear bands reported by Strehle & Stanley (1986) and Kim *et al.* (2007, 2011) are ductile structures that locally developed near the Hinesburg thrust and in other discrete zones in the hanging wall. They are approximately parallel to the D_1 foliation in the surrounding rocks (and to the thrust) and, according to Strehle & Stanley (1986), represent thrust reactivation. In zones of D_2 development that are far from the surface expression of the Hinesburg thrust, the D_2 cleavage is defined by mica-rich zones in phyllites or alternating quartz and mica domains in phyllitic quartzites, that truncate the D_1 foliation. Pressure solution and dislocation creep in quartz were the mechanisms of deformation during D_2 development (Strehle & Stanley 1986).

In the exposed parts of the footwall of the Hinesburg thrust, west of the thrust front, bedding is the dominant planar structure in sedimentary rocks. In addition, D_1 bedding-parallel thrusts were occasionally observed, some with slivers of adjacent lithologies. Reclined and rootless D_1 isoclinal folds of dolomitic layers were observed in black phyllites (OCsk) of the footwall. In the hanging wall, bedding was transposed into parallelism with the D_1 foliation, so it is not discussed separately.

Throughout the field area, both the hanging and foot walls of the Hinesburg thrust were deformed by orthogonal D_3 (north-striking) and D_4 (east-striking) folds, with steeply dipping axial surfaces, which superpose to form a map-scale (1:24 000) Ramsey (1967) Type-1 dome and basin interference pattern (Derman *et al.* 2008; Earle *et al.* 2010; Kim *et al.* 2011). As the metamorphic rocks in the hanging wall vary compositionally from phyllites to phyllitic quartzites (Fairfield Pond and Cheshire Formations), open-tight asymmetric folding of these units preferentially formed crenulation cleavage in the former and disjunctive/fracture cleavage in the latter. In the Town of Williston, which is in the northern half of the field area (see Fig. 1), rose diagrams and equal area nets (Fig. 4) show that both the D_3 and D_4 cleavages are steeply dipping and dominantly strike north–south (11°, 180°) and east–west (100°, 281°) (not considering standard deviations), respectively. The rose diagrams presented on this figure account for dip, using the right-hand rule.

At the map scale, the D_3 cleavage planes described above are parallel to the topographic lineaments that are formed by north–south trending, steep-sided, and narrow valleys on the LIDAR-based slope map of Fig. 5 (see Fig. 1A for

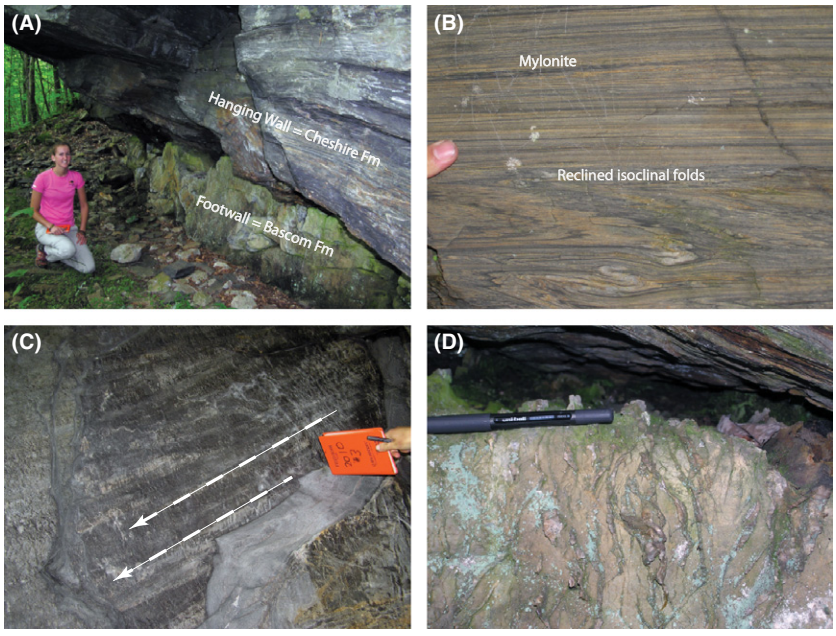

Fig. 3. The Hinesburg thrust at Mechanicsville (A) view of the thrust surface with phyllitic quartzites of the Cheshire formation in the hanging wall and dolostones of the Bascom formation in the footwall, (B) D_1 Mylonites (upper half) and reclined isoclinal folds (lower half) approximately 1 meter above thrust surface in the hanging wall, (C) D_1 stretching lineations in the hanging wall that are parallel to the motion direction of the thrust (upper right to lower left in the photo) and the axes of the D_1 reclined isoclinal folds, which have sheath fold geometry, (D) Dolostone of the footwall with multiple generations of quartz veins that are at varying angles to the thrust surface (above the pen in the upper third of the photo).

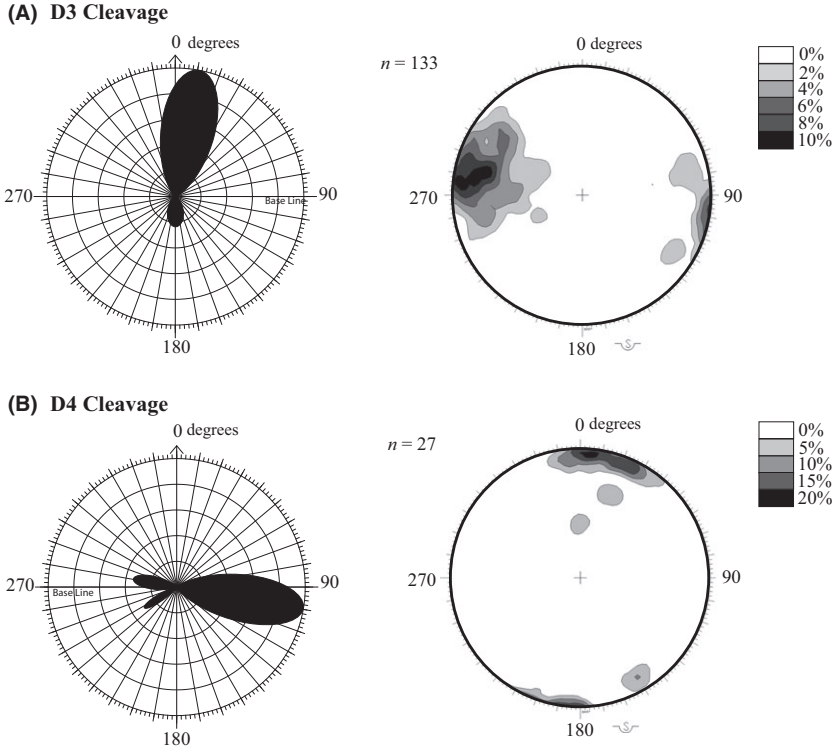

Fig. 4. Frequency-azimuth rose plots and contoured equal area nets (Daisy software, Salvini *et al.* 1999) of (A) D_3 and (B) D_4 cleavages in the Town of Williston (Kim *et al.* 2007, 2011). See text for explanation.

location). Based on field correlation, these lineaments occur on D_3 fold limbs in the hanging wall and are genetically related to the axial planar D_3 cleavage.

Detailed D_5 fracture analysis was completed in the hanging and foot walls of the Hinesburg thrust (Fig. 6) (Kim *et al.* 2007, 2011) in Williston (see Fig. 1A for location). The contoured equal area nets show that all fracture sets are steeply dipping. The dominant fracture azimuths for both hanging wall and footwall are (not considering standard deviations) east–west (84°, 290°) and north-north-east-south-southwest (22°, 232°) (Fig. 6A). East–west azimuths (92°, 283°) are dominant in the hanging wall

Fig. 5. Portion of the hanging wall of the Hinesburg thrust (see Fig. 1A for location) with bedrock geologic map of Kim *et al.* (2007) overlaying a gray-scale slope map (the steeper the slope, the darker the gray) derived from LIDAR data (Springston 2008). Note the abundance of approximately north–south trending topographic lineaments. Some of these lineaments are identified. These were correlated in the field with the D_3 cleavage that is axial planar to D_3 folds.

(Fig. 6B), whereas northeast-southwest azimuths (38°, 236°) are more pervasive in the footwall (Fig. 6C). Some of the east–west fracture sets have *en echelon* geometry. At the Mechanicsville site, both east-west and north-northeast to south-southwest trending fracture sets clearly cut through the hanging wall mylonites to the fault plane (Fig. 7).

All D_5 extension fracture sets were locally intruded by syn–post-extensional lamprophyre dikes that have been isotopically dated as Cretaceous in age (e.g., Armstrong & Stump 1971; McHone & Corneille 1980). Some north-northeast to south-southwest trending fractures are filled with quartz or quartz and carbonate (Strehle & Stanley 1986).

Well-log data

Whereas bedrock mapping and structural analysis accurately portray the surface expression of the Hinesburg thrust, the analysis of lithologic logs for bedrock groundwater wells constrains the third dimension. A domestic well-log database at the Vermont Department of Environmental Conservation (VDEC) was searched for logs that indicate an abrupt transition from phyllites and phyllitic quartzites of the hanging wall to carbonates and/or black phyllites characteristic of the footwall. The locations of these wells were correlated either with accurate street addresses (e911 emergency responder system) or with Global Positioning System (GPS) locations. In addition, two wells were logged in the field by the first author.

The 22 well logs show the Hinesburg thrust that was penetrated at depths that ranged from 65 to 300 m (Table S1). Figure 8A shows the location of nine wells on a geologic map that were drilled through the Hinesburg thrust, with eight of them projected onto cross-section A-A′ (Fig. 8B). These thrust wells, along with wells that did not penetrate the Hinesburg thrust, were used to construct cross-section A-A′ which shows that the thrust was deformed by D_3, large amplitude, asymmetric folds with approximately north–south striking and steeply east-dipping axial surfaces (e.g., Kim *et al.* 2007, 2011; Derman *et al.* 2008). In addition to the cross-sections, kilometer-scale folds can be seen on the LIDAR-based slope map (darkest shades represent the steepest slopes and *vice versa*) that underlies the bedrock geologic map of Fig. 8A; these folds were documented in the field by Kim *et al.* (2007) and Derman *et al.* (2008). Cross-section B-B′ also used water well logs to constrain the thrust depth (Fig. 8C) (see Fig. 1A for location).

Well logs from two closely spaced wells on Fig. 8A illustrate how the D_3 folds deform the Hinesburg thrust (wells W40465 and W38073). A detailed lithologic log, based on well cuttings, was constructed for well W40465 (Fig. 8A, B), where the Hinesburg thrust was encountered near the crest of a fold at a depth of 145 m. During the drilling of this well, the markedly slower penetration rate in an approximately 10-m-thick zone above the abrupt change to sedimentary rocks was attributed to the mylonite zone shown in Fig. 3B. Below the thrust, shaly limestones were encountered followed by black shales, with the only water-producing interval at this contact. On the far eastern limb of the same fold, well W38073 (Fig. 8A,B) showed the thrust at 290 m, at an abrupt transition from phyllites to carbonates; this interpretation was based on a geophysical log (gamma, not shown).

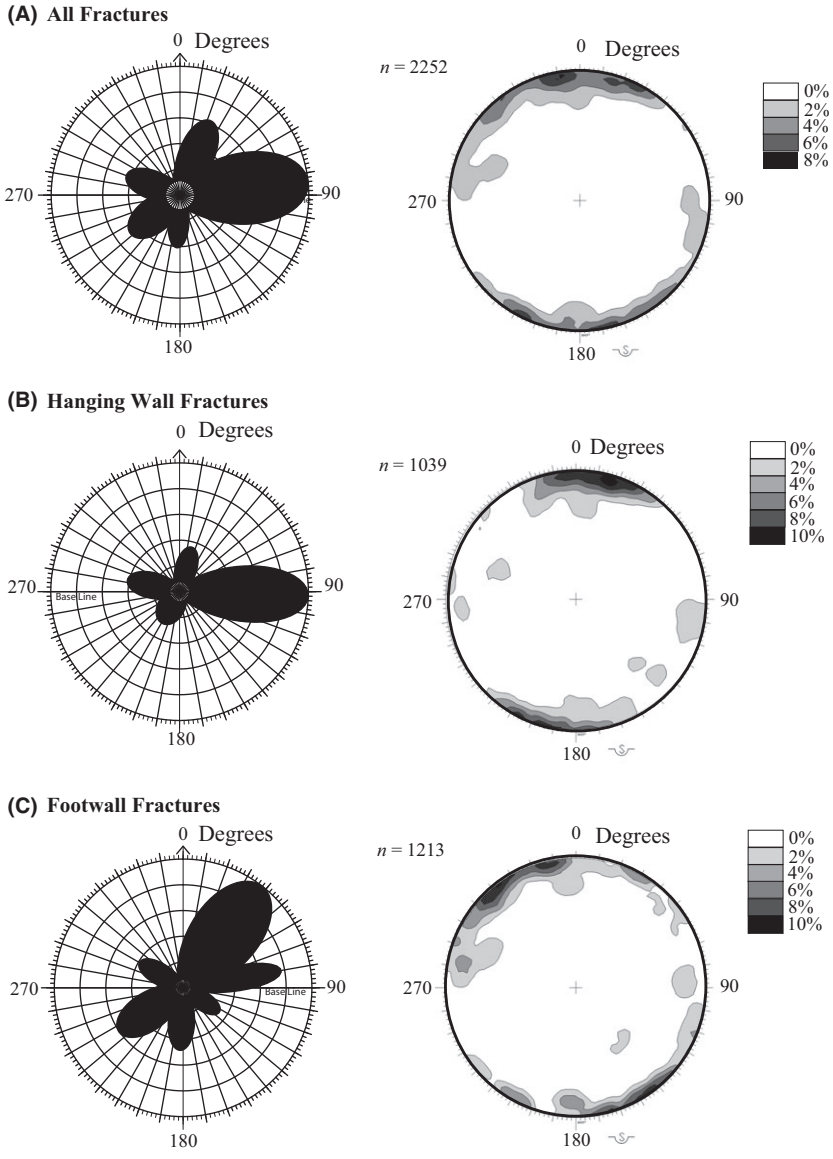

Fig. 6. Frequency-azimuth rose plots and contoured equal area nets (Daisy software, Salvini *et al.* 1999) of D_5 fractures in the Town of Williston (Kim *et al.* 2007, 2011). (A) fractures in both the hanging wall and footwall, (B) fractures in the hanging wall only, and (C) fractures in the footwall only. See text for explanation.

HYDROGEOLOGY

The physical hydrogeology of the area surrounding the thrust fault was synthesized from the previously cited Vermont Department of Environmental Conservation well-log database (depths, yields, and static water levels). Yields were determined from well driller yield tests that use compressed air from the drill rig to push groundwater from the well to the surface so that an approximate flow rate/yield can be measured (e.g., Massachusetts Department of Environmental Protection [http://www.mass.gov/eea/docs/dep/water/drinking/alpha/i-thru-z/wellyld.pdf]). For public water supply wells in Vermont, direct comparisons between well driller's yield tests and formal pumping tests by the Drinking Water and Groundwater Protection Division at the Vermont Department of Environmental Conservation showed that, on average, the driller's yield tests tend to overestimate the actual yield by a factor of two (R. Pingree, personal communication, 2013) In contrast, well driller yield tests have been used in other studies of fractured bedrock aquifers (e.g., DeSimone & Barbaro 2012), where they have been found to produce results similar to those of long-term pumping tests and do not contribute systematic bias. For simplicity, we used the well driller yield values at face value.

Using static water level and elevation data for bedrock wells throughout most of the field area, Filoon (2012) constructed reconnaissance-level piezometric contours for groundwater in the bedrock aquifer at a 50 m contour interval. Using these contours, generalized flow directions for the bedrock aquifer are shown in Fig. 9. The Lake Iroquois valley is a topographic low on the hanging wall that

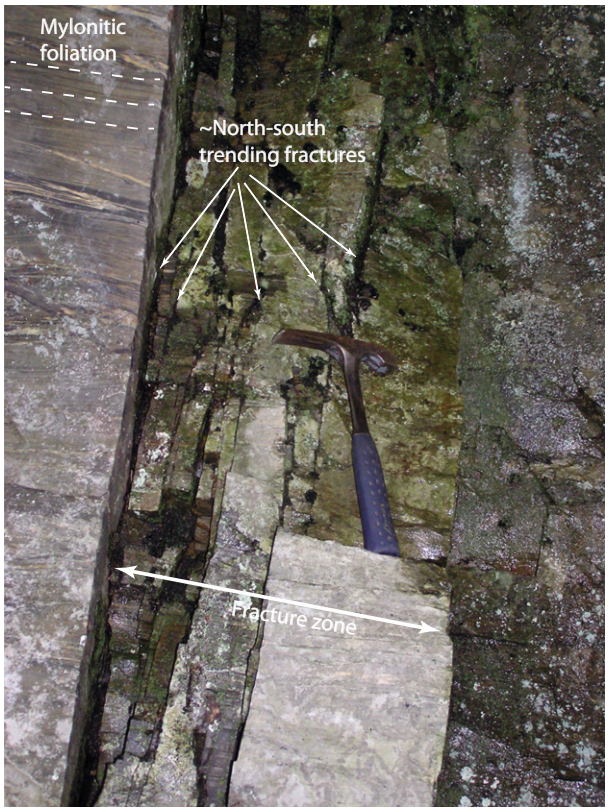

Fig. 7. North–south trending D_5 fracture zone that crosscuts the D_1 mylonitic foliation (dips gently to the right) at the Mechanicsville exposure of the Hinesburg thrust. A small bedrock spring emanates from this and other fractures. These and other D_5 fractures likely provide a hydraulic connection between the hanging wall and footwall aquifers.

roughly divides it into two parts. Based on the surface water flow directions shown in Fig. 9, this valley drains southward for most of its length and then turns southwestward and crosses onto the footwall. North of Lake Iroquois, there is a drainage divide where surface water flow changes from southward to northward. In the eastern part of the hanging wall, groundwater flow in the bedrock aquifer is dominantly to the west. In the western part of the hanging wall, flow is radially away from topographic highs and/or westward toward the footwall. Near the surface trace of the Hinesburg thrust, groundwater flow is consistently westward. In the footwall aquifer, groundwater flow directions are generally radially or laterally away from local topographic highs, which are comprised of more erosion-resistant bedrock, and toward topographic lows, like Shelburne Pond.

Well logs for 79 bedrock wells, including the wells sampled in this study ($n = 51$), were used to constrain cross-sections (Table S1). When the completion depths of wells drilled through the Hinesburg thrust are compared with the depths to the thrust, it is apparent that most of these wells were completed a significant depth below the thrust surface; therefore, all of the well data were grouped according to the units in which they were completed, as Type I footwall wells ($n = 22$), Type II hanging wall wells ($n = 34$), and Type III wells drilled through the Hinesburg ($n = 21$). Type III wells were further subdivided into wells completed <30 m below the fault ($n = 5$) (Type IIIA) and wells drilled through thrust to footwall wells and completed >30 m below the fault ($n = 16$) (Type IIIB) (Fig. 10A).

The well yield and well depth statistics for each group described above are shown through box and whisker plots in Fig. 10B,C. The box limits represent the median 50% of data values (2nd and 3rd quartiles), whereas the lines depict the maximum data range. Yields for wells completed in the three main lithotectonic zones footwall (Type I), hanging wall (Type II), and thrust (Type III) are also numerically presented on cross-section A-A′ (Fig. 8B). The highest median well depth range is associated with hanging wall (Type II) (108–305 m) and thrust wells (IIIA = 114–291 m, IIIB = 166–351 m, IIIA + IIIB = 144–339 m), whereas that of footwall wells (73–141 m) is considerably less (Fig. 10B). The median yield range for Type I footwall wells (5–102 lpm) and Type IIIB thrust wells (11–95 lpm) is very similar, in both cases, producing mainly from fractured sedimentary rocks of the footwall. Bedrock wells completed in the metamorphic rocks of the hanging wall of the Hinesburg thrust have very low median yield ranges (1–9 lpm), compared with those completed in any other lithotectonic zone. For wells drilled through the Hinesburg thrust, Type IIIA wells (87–237 lpm) have a considerably higher median yield range than Type IIIB wells (11–95 lpm). Type IIIB wells were completed <30 m below the Hinesburg thrust.

Static water levels are only available for seven of the 22 wells in the field area that penetrated the Hinesburg thrust (Table S1). Although these measurements do not necessarily represent an equilibrium piezometric surface, they show water levels that rose tens of meters above the thrust level in the borehole directly after the well was completed. However, taken in context, Filoon (2012) found that the static levels of hanging wall wells are greater than the static levels of thrust wells by an average of 20 m, suggesting a general downward hydraulic gradient.

Filoon (2012) obtained reconnaissance CFC-11, CFC -12, and CFC -113 apparent recharge ages on groundwater from nine bedrock wells in the field area (Table 2). The apparent ages of groundwater in thrust wells (approximately 40 years) compared with hanging wall and footwall wells (approximately 30 years) are similar enough to indicate that groundwater is predominantly modern in the footwall, hanging wall, and thrust zone. For CFC methods, statistics, and the full dataset, refer to Filoon (2012).

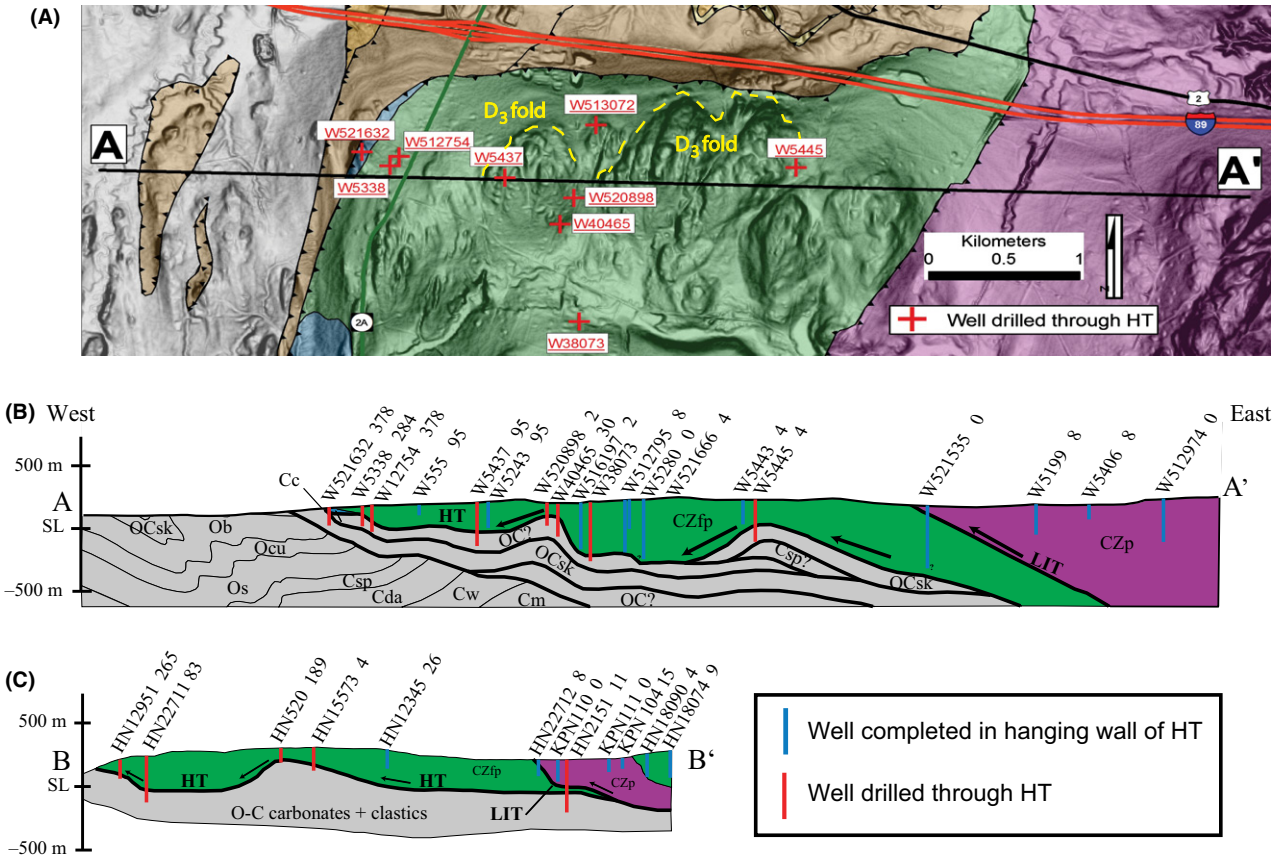

Fig. 8. (A) Bedrock geologic map of Kim *et al.* (2007) in the vicinity of cross-section A-A′, which overlays a grayscale slope map (the steeper the slope, the darker the shade of gray) derived from LIDAR data (Springston 2008); red crosses mark the locations of wells drilled through the Hinesburg thrust; dashed yellow lines outline mapped D_3 folds. (B) Northern cross-section A-A′; note the large amplitude D_3 folds that deform the thrust, as determined from the analysis of water well logs; labels above each well first give well number and then well yield (liters per minute (lpm), note that wells drilled through the thrust generally have significantly higher yields that those completed in the hanging wall; see text for details. For simplicity, all lithologies in the footwall are colored gray; the labels for the lithologies can be correlated with those in Fig. 1. (C) Southern cross-section B-B′ that also shows map-scale D_3 folds, based on well logs. HT = Hinesburg Thrust, LIT = Lake Iroquois Thrust. The locations of cross-sections A-A′ and B-B′ are shown on Fig. 1A.

AQUEOUS AND BEDROCK GEOCHEMISTRY

The source of the elevated radioactivity was evaluated by testing groundwater from bedrock wells and by analyzing compositions of bedrock from local outcrops. Fifty-one groundwater samples were collected from wells of Types I through III; sampling details are provided in the data repository (Table S2). Groundwater samples were analyzed for gross alpha radiation and U at the Vermont Department of Health and Laboratory in Burlington, Vermont. Concentrations of metals and anions were analyzed at the Vermont Department of Environmental Conservation Laboratory in Waterbury, Vermont. Details of analytical methods and precision are presented in the Supporting Information (Table S3). Seventy-three bedrock samples from the formations that comprise the regional aquifer were collected from outcrops and analyzed for whole-rock geochemistry by a combination of inductively coupled plasma mass spectrometry (ICP-MS) and ICP-atomic emission spectrometry (ICP-AES) following fusion with $LiBO_2$. Details of sample preparation and analytical precision are presented in the Supporting Information (Table S4). We will now present major element, radionuclide, and trace element groundwater geochemical data for the different lithotectonic groups. A summary of the groundwater geochemical data is shown in Table 3, and all of these data are in Table S5. These data are derived from North (2005), Davis (2008), and Bean (2009).

Piper diagrams

Groundwater from Type I wells in the footwall west of the thrust front has a strong Ca-Mg-HCO_3 signature, whereas Type II (hanging wall) groundwater spans a compositional spectrum intermediate between Na+K-Cl and Ca-Mg-HCO_3 end members (Fig. 11). Notably, groundwater in the footwall below the thrust fault (Types IIIA and IIIB wells) plots similar to Type II wells.

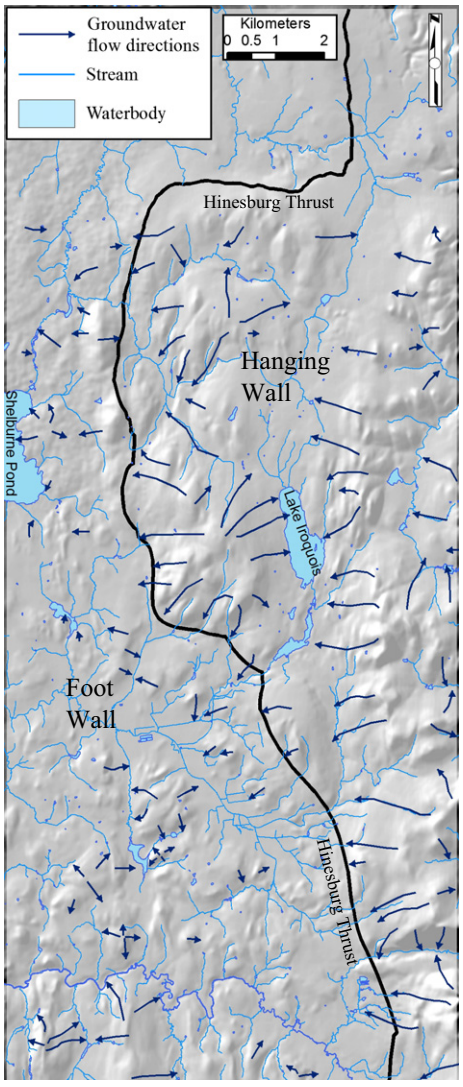

Fig. 9. Generalized groundwater flow directions for the bedrock aquifer in the field area based on piezometric surface contours drawn by Filoon (2012) at 50 m intervals. Streams and lakes are also shown so that surface water flow directions can be inferred.

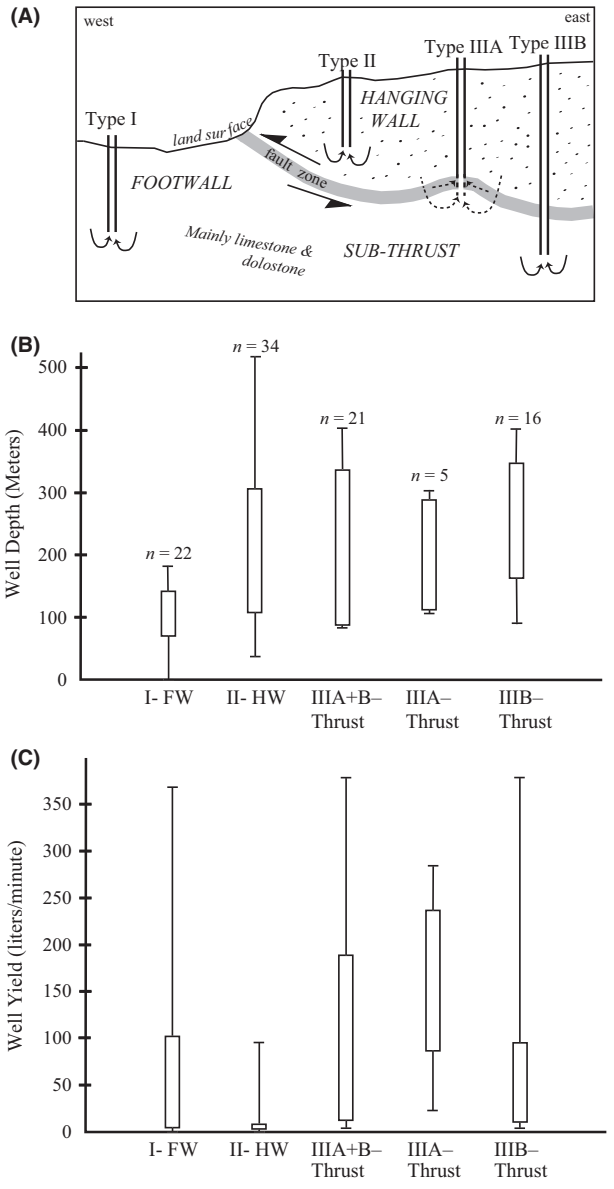

Fig. 10. (A) Schematic diagram of the four main bedrock well types in the field area, Type I – footwall well west of the thrust front, Type II – hanging wall well, Type IIIA – completed <30 m below thrust, Type IIIB – completed >30 m below thrust. Box and whisker plots showing second and third quartiles (boxes) and minimum and maximum range of data (whiskers) for (B) well depths and (C) well yields for each well type. Note that the data for Type IIIA and Type IIIB wells are shown together and separately. See text for details.

Radionuclides

Gross alpha radiation, which is the total alpha radiation emitted by radiogenic species in groundwater such as uranium and radium, is commonly used as a screening test for determining health risk and recommending further testing. In Vermont, one of the common screening limits is 15 picocuries liter^{-1} (pCi l^{-1}), beyond which further testing for ^{226}radium, ^{228}radium, and uranium is recommended. We determined gross alpha and uranium results for groundwater from all sampled bedrock wells and then collated these data by lithotectonic unit in Table 4 to look for trends.

Mean gross alpha levels for wells that were completed either in the hanging wall of the Hinesburg thrust or drilled through the thrust into the footwall are approximately three times greater than the levels from wells drilled into the footwall west of the thrust front. As a whole, 50% of Type III wells have elevated gross alpha, and the same percentages hold for Type IIIA and Type IIIB wells, when considered separately. There are also notable differences in Type II wells based on well lithology, for example, 67% (6 of 9) wells in the Pinnacle formation exceed 15 pCi l^{-1},

Table 2 Recharge ages (in years before present) based on concentrations of three chloroflurocarbons. Given the lack of contamination in CFC-11 dates relative to CFC-12 and CFC-113, CFC-11 dates were used to assess groundwater ages (right column). Ages could not be determined for samples in cases where samples were supersaturated (SS) or obscured (OBS). Analysis was performed by Tritium Labs of the Rosenstiel School of Marine and Atmospheric Science, University of Miami, Florida, USA

Type	Sample ID	Rep	CFC-11	CFC-12	CFC-113	AGE
II (hanging wall)	KPN-104	1	34 ± 2	SS	26 ± 2	26 ± 2
		2	33 ± 2	SS	26 ± 2	
		3	33 ± 2	SS	26 ± 2	
II (hanging wall)	062207-3	1	40 ± 2	SS	31 ± 2	31 ± 2
		2	40 ± 2	SS	31 ± 2	
		3	40 ± 2	SS	31 ± 2	
II (hanging wall)	KPN-107	1	36 ± 2	SS	26 ± 2	27 ± 2
		2	36 ± 2	SS	27 ± 2	
		3	35 ± 2	SS	27 ± 2	
III-B (thrust)	72507-7	1	53 ± 2	49 ± 2	41 ± 2	42 ± 2
		2	54 ± 2	54 ± 2	43 ± 2	
		3	50 ± 2	49 ± 2	41 ± 2	
III-B (thrust)	KPN-102	1	47 ± 2	43 ± 2	36 ± 2	37 ± 2
		2	48 ± 2	45 ± 2	37 ± 2	
		3	48 ± 2	46 ± 2	37 ± 2	
III-B (thrust)	KPN-105	1	37 ± 2	OBS	37 ± 2	37 ± 2
		2	ND	ND	ND	
		3	ND	ND	ND	
I (footwall)	101408-5	1	28 ± 2	14 ± 2	24 ± 2	23 ± 2
		2	27 ± 2	SS	23 ± 2	
		3	27 ± 2	SS	23 ± 2	
I (footwall)	102708-9	1	54 ± 2	45 ± 2	41 ± 2	41 ± 2
		2	54 ± 2	45 ± 2	41 ± 2	
		3	54 ± 2	45 ± 2	42 ± 2	
I (footwall)	110308-13	1	SS	20 ± 2	25 ± 2	25 ± 2
		2	SS	20 ± 2	25 ± 2	
		3	SS	17 ± 2	25 ± 2	

and the average gross alpha concentration is 33 pCi l^{-1}. By comparison, only 7% (1 of 14) of Type II wells in the stratigraphically higher (younger) Fairfield Pond formation exceed 15 pCi l^{-1}, and average gross alpha concentration is only 8.7 pCi l^{-1}. None of the three wells in surficial deposits exceed 2 pCi l^{-1}.

Uranium concentrations generally follow gross alpha radiation trends with respect to structural unit: 16% of Type II wells (4/25) exceed the Vermont maximum contaminant level of 20 μg l^{-1} and 25% (1/4) of Type IIIB (well completed >30 m below the thrust) wells exceed 20 μg l^{-1}, while no Type IIIA (0/2) or Type I (footwall) wells (0/20) exceed 20 μg l^{-1}. Average U concentration in hanging wall groundwater is 17.2 μg l^{-1}, and as with alpha radiation, this elevated signature is dominated by groundwater produced from the Pinnacle formation, where 33% of wells exceed 20 μg l^{-1}, average U is 30.9 μg l^{-1}, and the maximum value is 143 μg l^{-1}.

Gross alpha and uranium levels for all lithotectonic well categories are shown in Fig. 13A,B. It is notable that all elevated gross alpha (>15 pCi l^{-1}) and uranium (>20 μg l^{-1}) occur either in wells completed in the hanging wall (Type II) or drilled through the Hinesburg thrust (Types IIIA and IIIB) (Fig. 12A,B). If the thrust well types are examined separately, Type IIIA ($n = 2$) and IIIB ($n = 4$) wells have one elevated gross alpha and zero elevated uranium occurrences, and two elevated gross alpha occurrences and one elevated uranium occurrence, respectively. For wells competed in the hanging wall or drilled through the thrust, the elevated gross alpha incidences (10) are double that of elevated uranium, which indicates a source of alpha radiation other than that derived from the radioactive decay of uranium. By testing six hanging wall and thrust wells for ^{226}Ra and ^{228}Ra (Table S5), ^{226}Ra was determined to the missing isotope; ^{228}Ra is not an alpha particle emitter.

In the absence of radium tests, residual gross alpha (RGA) provides a means of generally expressing the quantity of alpha radiation that is *not* produced by uranium decay. It is calculated according to the equation (EPA 2000):

$$\alpha\,\text{residual}\,(\text{pCi}\,l^{-1}) = \text{gross alpha}\,(\text{pCi}\,l^{-1}) - (0.67 \times [\text{U}])$$

RGA can be used as a proxy for the abundance of ^{226}Ra. In addition, the ratio of residual gross alpha to total gross alpha gives an approximation of the ratio of radium-derived alpha radiation to total alpha radiation. RGA levels and RGA/TGA ratios were calculated for all lithotectonic well categories (Fig. 12C and Table S5). The fact that 39% of all hanging wall and thrust wells have RGA/TGA ratios >0.50 indicates that radium may comprise a significant portion of the gross alpha total.

Multielement plots

To discriminate further between groundwater from Type I versus II versus III wells, gross alpha, Na, Mg, Ba, Sr, and alkalinity were chosen as parameters because together they provide compositional fingerprints of hanging wall versus footwall groundwater (Fig. 13). Figure 13A,B is box and whisker spider plots for footwall (Type I) and hanging wall (Type II) wells, respectively, using these parameters. To have all these parameters display within the same range on these plots, Ba, Sr, and alkalinity were divided by the same constants for the two well types. Whereas the footwall wells have higher median Mg and alkalinity, the hanging wall wells have higher median gross alpha, Na, Ba, and Sr. Using Fig. 13A,B as references, we will now evaluate the groundwater composition of thrust wells.

Figure 14A shows the six Type III wells that were sampled for groundwater chemistry in this study. The wells are arranged from west to east based on the distance each well is located from the Hinesburg thrust front and labeled whether it is considered Type IIIA (completed <30 m below the thrust) or Type IIIB (completed >30 m below the thrust); lithologies are also shown. Spider plots for these thrust wells were constructed using the same parameters as above and are directly compared with Fig. 13A,B by using dashed lines for footwall wells (Type I) and solid

Table 3 Composition of groundwater in bedrock wells producing from the footwall (Type I), hanging wall (Type II), and wells drilled through the Hinesburg thrust (Type III). The right-hand column indicates predominant control on composition of groundwater in Type III wells, where 'HW' = hanging wall signature, 'FW' = footwall signature, and 'Mixing' = influence of both HW and FW. 'Depth' indicates parameters whose values are largely controlled by the depth of Type III wells. 'Anthro' = likely anthropogenic influence. 'HW' and 'Mixing' signatures are evidence for flow of groundwater through fractures that cross-cut the thrust.

		Footwall (Type I, dominantly carbonates)				Hanging wall (Type II, dominantly siliciclastic)				Thrust wells (Type III)				
		N = 20				*N* = 25				*N* = 6				
Variable	Unit	Mean	SD	Min	Max	Mean	SD	Min	Max	Mean	SD	Min	Max	Signal
Alpha	pCi l^{-1}	7.0	*4.1*	1.3	13.7	18.3	*25.0*	1.1	107	18.6	*13.3*	3.7	39.8	HW
U	ppb	4.3	*3.0*	<1	9.7	17.2	*33.4*	<1	143	7.0	*7.2*	2.3	20.4	Mixing
Temp	°C	10.1	*0.8*	9.2	12.9	11.0	*1.2*	9.0	13.1	11.5	*1.5*	10.3	14.4	Depth
Cond	ms	504	*166*	218	807	495	*539*	238	1780	296	*117*	200	512	Depth
DO	%	27.1	*22.8*	5.8	68.0	37.0	*19.8*	7.4	84.1	22.9	*21.8*	9.5	65.7	Depth
pH		7.3	*0.4*	6.4	8.1	8.0	*0.6*	7.2	9.4	8.0	*0.6*	7.1	8.6	HW
ORP	mV	117	*72*	11	243	116	*64*	−93	202	129	*43*	51	184	Neither
Na	ppm	6.0	*4.6*	0.7	16.6	25.7	*22.2*	3.2	90.0	24.5	*9.4*	8.0	34.0	HW
Mg	ppm	31.7	*10.5*	9.3	44.4	10.6	*8.7*	<1	37.1	10.8	*11.9*	0.8	33.3	HW
K	ppm	0.9	*0.7*	0.5	3.6	0.7	*0.5*	0.2	2.3	0.4	*0.2*	0.3	0.7	Neither
Ca	ppm	67.4	*24.0*	29.0	123	45.3	*23.2*	12.1	123	22.4	*16.5*	9.7	54.9	Neither
Alkalinity	ppm	256	*80*	92	432	150	*48*	80	269	200	*76*	146	253	Mixing
SiO_2	ppm	10.0	*3.1*	4.2	16.6	14.3	*2.4*	11.2	20.3	13.3	*4.2*	10.3	16.2	Mixing
Fe	ppm	1.8	*5.2*	<0.05	22.2	0.19	*0.43*	<0.05	2.2	<0.05	–	<0.05	<0.05	Neither
Mn	ppb	43.7	*91.7*	<5	378	14.1	*17.9*	<5	78.9	<5	–	<5	<5	Neither
Cl^-	ppm	8.0	*8.4*	0.36	24.0	39.0	*64.2*	<0.1	178	4.2	*4.4*	1.1	7.4	Anthro
NO_3	ppm	0.68	*1.2*	<0.1	4.6	0.19	*0.3*	<0.1	1.4	<0.1	–	<0.1	<0.1	Anthro
P	ppb	25.8	*9.4*	<5	32.6	8.7	*5.1*	<5	22.3	7.3	*1.3*	6.3	8.2	Anthro
SO_4	ppm	22.7	*13.3*	2.3	50.6	31.3	*11.4*	18.7	60.1	27.8	*6.3*	23.3	32.2	Mixing
As	ppb	1.6	*1.0*	<5	3.9	3.7	*4.6*	<1	20.9	1.6	*0.7*	<1	2.6	FW
Ba	ppb	41.6	*34.9*	<5	147	95.0	*51.5*	33.9	171	62.3	*17.0*	28.3	74.4	Mixing
Cu	ppb	11.1	*5.1*	<10	32.6	76.0	*276.5*	<10	1400	20.7	*18.3*	<10	56.8	Mixing
Sr	ppb	196	*152*	59.0	701	2363	*1746*	481	7790	2640	*921*	1260	3970	HW

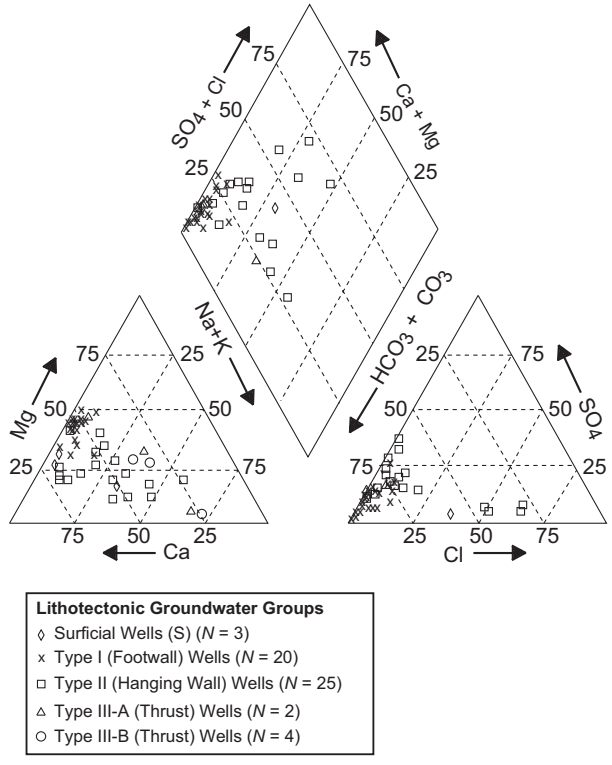

Fig. 11. Piper Plots of groundwater from each well type (Piper 1944).

lines for hanging wall wells (Type II). The following observations were made regarding the groundwater chemistry of Type III wells: (i) Wells 72507-7 (Fig. 14C), KPN102 (Fig. 14D), KPN105 (Fig. 14E), and KPN106 (Fig. 14G), which are all considered Type IIIB, clearly have a hanging wall signature; (ii) Well 80607-2 (Fig. 14B), a Type IIIA well, shows higher gross alpha and Ba, characteristic of the hanging wall, but lower Na and Sr, and higher Mg and alkalinity, characteristic of the footwall; (iii) Although the lower gross alpha, Ba, and Mg in well KPN101 (Type IIIA) may reflect median footwall abundances, the higher Na and Sr are consistent with median hanging wall abundances. In summary, Type IIIB wells have a groundwater geochemical signature with hanging wall affinity, whereas Type IIIA wells can be interpreted to have some degree of mixed signature between the hanging wall and footwall.

Whole-rock geochemistry

Box and whisker plots were also used to display the whole-rock geochemistry of lithologies in the hanging wall and footwall. Although Na, Mg, Ba, and Sr were also used to characterize whole-rock geochemistry signatures, U+Th and Ca were, respectively, substituted for the gross alpha and alkalinity parameters used with groundwater. Whole-

Table 4 Alpha radiation in groundwater from the three main lithotectonic units (hanging wall (Type I), footwall (Type II), and through thrust (Type III).

Well Type	Number of wells	Maximum gross alpha (pCi l^{-1})	Mean gross alpha (pCi l^{-1})	% wells exceeding 15 pCi l^{-1}	Maximum U (ppb)	Mean U (ppb)	% wells exceeding 20 ppb
Type I wells Footwall	20	13.7	6.7	0	9.7	4.1	0
Type II wells Hanging wall	25	107	18.3	36	143	17.2	16
Type IIIA wells	2	39.8	21.8	50	9.7	6	0
Type IIIB wells	4	24.1	17	50	20.4	7.4	25
Type III wells (All)	6	39.8	18.6	50	20.4	7	17

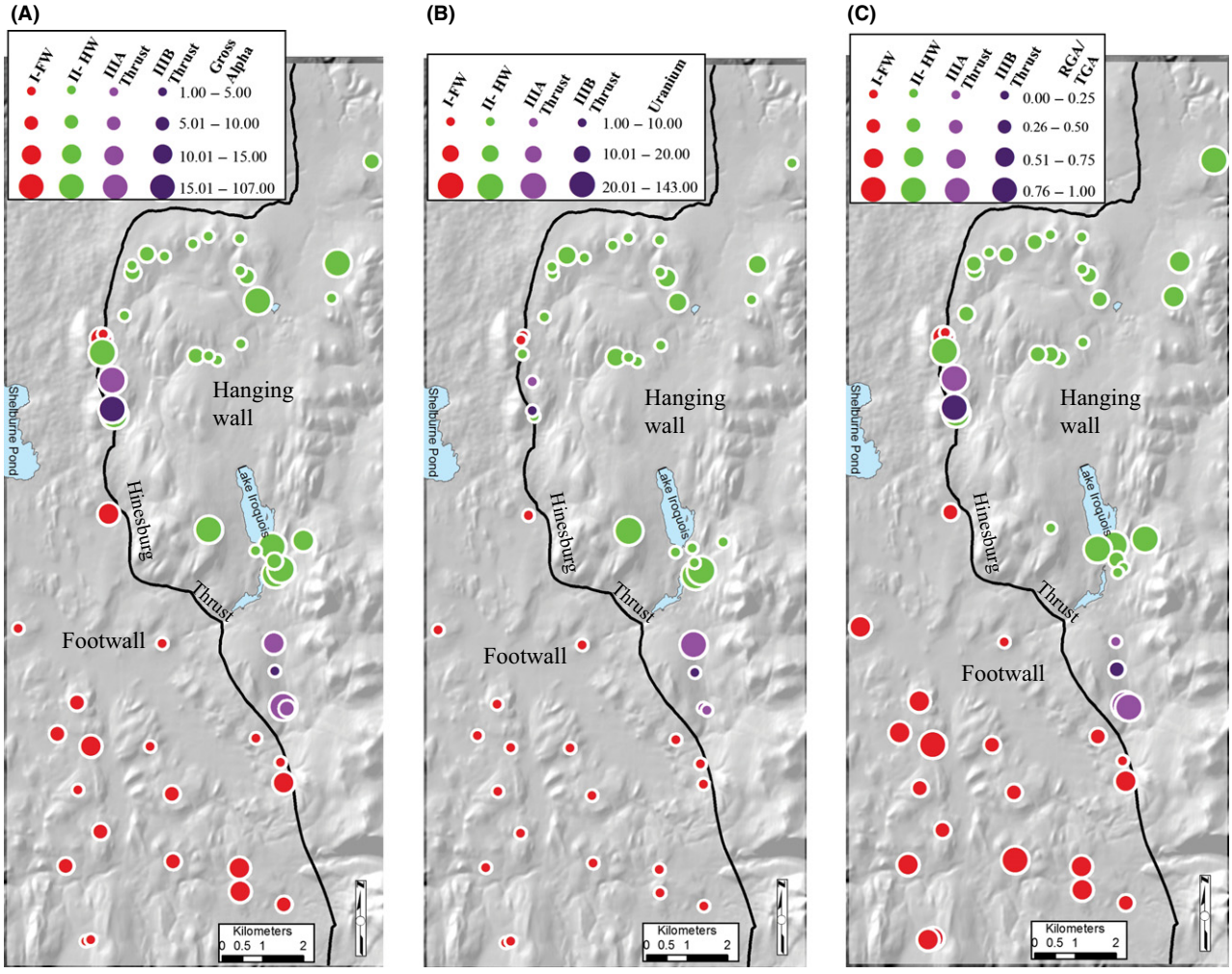

Fig. 12. Scaled (radius of symbol) gross alpha (A), uranium (B), and (C) residual gross alpha (RGA)/total gross alpha (TGA) abundances for each well type in the field area. FW = footwall, HW = hanging wall, gross alpha units are picocuries $liter^{-1}$, U units are parts per billion, RGA/TGA values are ratios.

rock chemical compositions of metamorphosed clastic-dominated hanging wall rocks are elevated in U+Th, Na, and Ba relative to footwall rocks, and higher Ca and Mg abundances are found in the carbonate-dominated footwall rocks (Table 5; Fig. 15). Whereas Table 5 is only a summary of the whole-rock data, the full dataset can be found in Table S6. These data are derived from North (2005), Davis (2008), and Bean (2009). With the exception of Sr, these signatures are very similar to those seen in the groundwater compositions of Fig. 13.

DISCUSSION

The architecture and permeability structure of upper crustal brittle fault zones are considerably different than that of ductile fault zones. For example, Chester & Logan (1986),

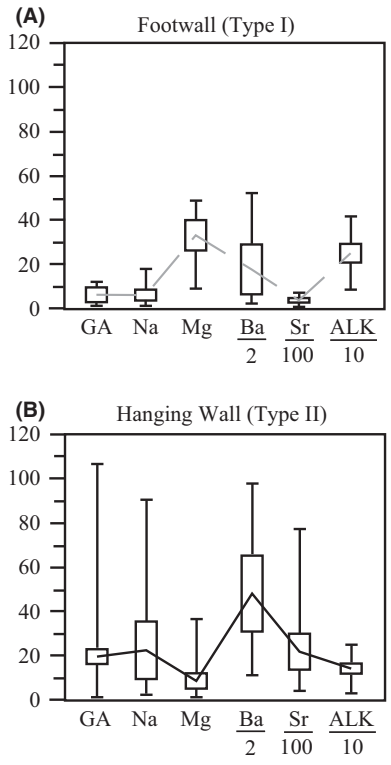

Fig. 13. Box and whisker spider plots showing second and third quartiles (boxes) and minimum and maximum range of data (whiskers) for groundwater geochemical data from (A) footwall (Type I) wells and (B) hanging wall (Type II) wells. See text for explanation. GA = gross alpha (picocuries liter^{-1}); Na, Mg, and ALK (alkalinity) in parts per million; Ba and Sr in parts per billion.

Bruhn *et al.* (1994), Caine *et al.* (1996, 2010), Gudmundsson (2011) and Bense *et al.* (2013) indicate that brittle upper crustal fault zones consist of three parts, which are (i) the fault core, the internal portions adjacent to the slip surface along which the highest strain and displacement occurred; (ii) the damage zone, the portions external to the fault core where the residual strain eventually diminishes moving outward; and (iii) the protolith, the unstrained rock on either side of the fault. In this type of fault scenario, fractures and minor faults are common in the damage zone whereas breccias and cataclastic rock dominantly comprise the fault core. Consequently, damage zones are generally conduits for groundwater flow, whereas the fault core tends to be a barrier.

In contrast, Caine *et al.* (2010) summarize the following points regarding the architecture and permeability structure of ductile fault zones: (i) They are frequently cored by highly strained mylonitic rocks that grade progressively outward on either side into less-strained rocks of the protolith; (ii) a damage zone *sensu stricto* is absent; (iii) the crystal plastic deformation associated with ductile shear zones maintains rock cohesion and inhibits the development of transmissive planar structures that are favorable for groundwater transport; and (iv) the mylonitic 'core' and protolith of a ductile fault zone may have similar permeabilities, unless the fault is active.

The Hinesburg thrust juxtaposes muscovite–biotite-grade metamorphic rocks (phyllitic quartzites) of the hanging wall with dominantly carbonate sedimentary rocks of the footwall. Based on the presence of D_1 mylonites, reclined isoclinal folds with sheath fold geometry, well-developed stretching lineations aligned with the fault transport direction, and superposed D_2 asymmetric shear bands in hanging wall metamorphic rocks and extensively recrystallized carbonates with bedding-parallel thrusts in the footwall, the Hinesburg thrust unequivocally represents a ductile fault zone that was active during the Ordovician Taconian orogeny. Because the mylonites deformed by the process of ductile flow (crystal plastic deformation) (e.g., Passchier & Trouw 2005), which maintains rock cohesion and prevents the development of planar structures, we would not expect them to be very permeable to groundwater (Caine *et al.* 2010). After a brief discussion of fault-related veins and their potential effect on fault zone permeability, the post-Ordovician tectonic evolution of this thrust will be discussed in detail.

There are multiple generations of pre and syn D_1 veins in the hanging wall at the Mechanicsville site, which recorded transient periods of brittle deformation. However, the quartz grains within these veins have been strongly overprinted by the D_1 and D_2 ductile structures and have strong shape and lattice-preferred orientation. These highly strained veins would not be permeable to groundwater flow.

Quartz and quartz-carbonate veins and stylolites in dolostones in the footwall of the Hinesburg thrust at Mechanicsville occur at all angles to the thrust surface. Strehle & Stanley (1986) propose that these veins formed during or after S_1 as metamorphic fluids permeated the thrust. The heavy veining and recrystallized fabric of the dolostone also suggest that this footwall lithology is probably not permeable. The fault surface at Mechanicsville is not sufficiently exposed to evaluate the lateral extent of the veins in either the footwall or hanging wall.

Depending on the lithology (phyllite versus phyllitic quartzite), the orthogonal D_3 and D_4 fold sets generated crenulation and disjunctive/fracture cleavages. At the outcrop scale, there is no visible secondary porosity associated with D_3 and/or D_4 crenulation cleavage. Although disjunctive cleavage planes locally looked like fractures, they were rarely open. There are also map-scale north–south trending topographic lineaments that are directly related to D_3 folding and its associated axial planar cleavage (Fig. 5), which presumably overprint the thrust surface. However, because these lineaments occur in sparsely populated rural areas, there is insufficient well coverage to evaluate their permeability structure. We do not consider D_3 and D_4

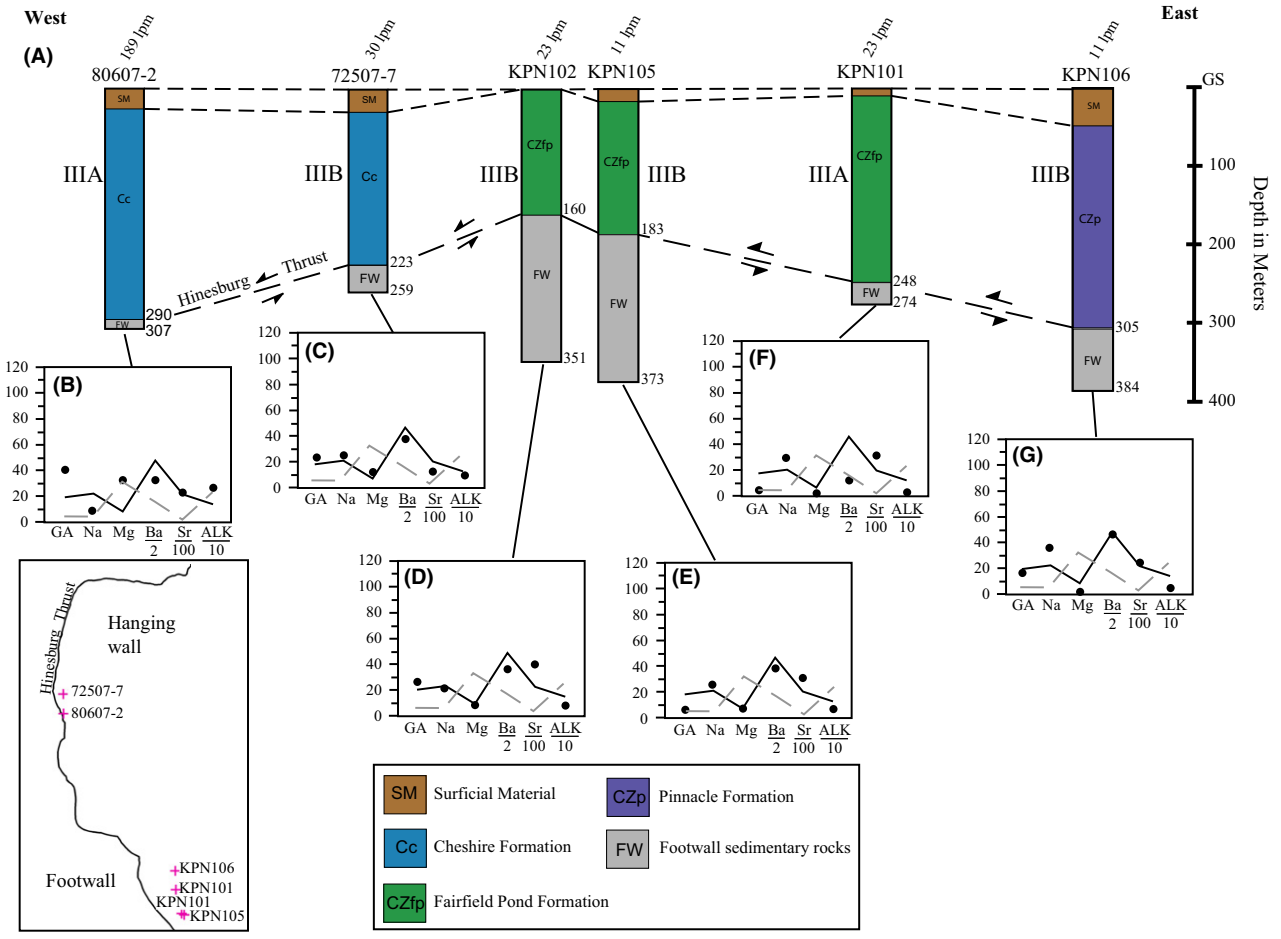

Fig. 14. (A) Lithologic logs for thrust wells (Type III) that were sampled for groundwater geochemistry; they are arranged from west to east based on their normal distance to the Hinesburg thrust front (see inset map). No vertical exaggeration. (B–F) show spider diagrams of the same geochemical parameters as Fig. 13. Solid and dashed lines are the hanging wall and footwall geochemical signatures, respectively. Well yields in liters per minute (lpm) are shown above each well.

cleavages to be viable pathways for groundwater flow, unless they localized later fracturing.

Figures 4 and 6 show rose diagrams and contoured equal area nets for D_3 and D_4 cleavages and D_5 extension fractures, respectively. The D_3 cleavage strikes approximately north–south, whereas D_4 strikes east–west; both dip steeply. Within error, there are two D_5 fracture sets of the same attitudes. We believe that it is possible that the D_3 and D_4 cleavages may have localized the formation of these two D_5 fracture sets. The orientations of fractures that form in previously deformed rocks are greatly affected by the orientations of preexisting planes of weakness, such as an inherited foliation or an older joint set. These mechanical anisotropies influence the shear strength of a rock in different directions and, therefore, influence the geometry of any new fracture sets (e.g., Donath 1961; Twiss & Moores 2007). It is possible, however, that the D_3 and D_4 cleavages are unrelated to any D_5 fractures.

D_5 extension fractures were conduits for fluid flow (magmas) during the Cretaceous because all dominant fracture sets in the field area were locally intruded by lamprophyres of this age (135–115 Ma; McHone 1978, 1987). These alkali rocks are of continental rift-zone tectonic affinity and are mantle-derived, so they must have risen upward along preexisting planes of weakness in the hanging and foot walls of the Hinesburg thrust.

At the Mechanicsville site, both approximately N-S and E-W trending, approximately vertical fracture sets cut through the mylonites of the hanging wall of the Hinesburg thrust and abut the fault surface. Some of the N-S fractures have *en echelon* geometry. In terms of modern groundwater flow, it is important to note that bedrock springs emanate from some N-S and E-W fractures, making these fractures groundwater conduits through the mylonites.

In summary, based on the examination of Ordovician D_1 and D_2 ductile structures alone, it cannot be said with any certainty whether the permeability of the fault zone of the Hinesburg thrust is any greater than the hanging wall and footwall protoliths on either side. However, subse-

Table 5 Geochemistry of rocks that are the dominant types in the footwall and hanging wall of the Hinesburg thrust fault. All data is presented in Table S6. Values are presented on anhydrous basis — major elements are wt % oxide, and trace elements are mg kg^{-1} (ppm).

		Footwall carbonates only (N = 21)				Hanging wall siliciclastics (N = 46)			
	DL	Mean	SD	Minimum	Maximum	Mean	SD	Minimum	Maximum
SiO_2	0.2	**17.2**	***16.4***	**<0.2**	**65.4**	**66.6**	***9.9***	**45.9**	**94.0**
TiO_2	0.01	0.15	*0.15*	<0.01	0.70	1.04	*0.41*	<0.1	2.42
Al_2O_3	0.05	1.75	*1.60*	0.42	7.77	17.0	*5.9*	1.82	32.1
Fe_2O_3	0.2	1.16	*0.73*	0.35	3.04	5.91	*2.11*	2.05	9.87
MnO	0.01	0.06	*0.05*	<0.01	0.18	0.07	*0.02*	0.01	0.12
MgO	0.01	**20.1**	***14.8***	**1.15**	**37.7**	**1.68**	***0.73***	**0.23**	**3.96**
CaO	0.01	58.7	*20.8*	19.6	93.7	0.92	*1.79*	0.08	12.08
Na_2O	0.01	**0.22**	***0.34***	**<0.01**	**1.28**	**2.23**	***1.16***	**0.40**	**5.19**
K_2O	0.05	0.63	*0.53*	0.12	1.93	4.47	*2.09*	0.27	9.80
P_2O_5	0.01	0.06	*0.07*	<0.01	0.27	0.12	*0.06*	<0.01	0.32
As	1.0	2.4	*1.8*	<1	7.0	4.6	*6.7*	<1	23
Ba	0.5	**118**	***148***	**13**	**533**	**858**	***383***	**50**	**1587**
Cu	0.1	**1.1**	***1.0***	**<0.1**	**4.4**	**13.0**	***6.6***	**3**	**30**
Pb	0.1	3.0	*1.7*	1.0	6.5	16.5	*17.7*	3	64
Sr	0.1	160	*97*	60	331	88	*48*	21.4	287
Th	0.1	0.6	*0.4*	0.1	1.5	12.6	*6.0*	0.9	30.3
U	0.05	**1.6**	***1.6***	**0.1**	**5.3**	**2.6**	***1.2***	**0.1**	**6.7**
Zn	1.0	11.9	*10.5*	1.0	37.0	82.7	*47.6*	11	310

Bold and italic values indicate bedrock components that appear in groundwater compositions as evidence for mixing of HW (Type II well) groundwater and thrust (Type III well) groundwater (Table 3). DL = detection limit; SD = standard deviation. Complete data set is in Table S6.

quent Devonian D_3 and D_4 events folded the thrust and produced cleavages that may have localized some D_5 Cretaceous extension fracture sets, which enhanced the hydraulic connection between hanging wall and footwall. It is also possible that the D_3 and D_4 cleavages are independent of the later fracture development.

Subsurface physical hydrogeology

The box and whisker plots on Fig. 10C highlight the large difference in median yield between bedrock wells completed in metamorphic rocks of the hanging wall of the Hinesburg thrust (low) versus those completed in carbonate sedimentary rocks of the footwall (high). Whether a well is completed in the footwall west of the thrust front (Type I) or significantly below (>30 m) the thrust (Type IIIB), the median yields displayed by the boxes (2nd and 3rd quartiles) and low and high ranges are very similar (Fig. 10C). Therefore, in terms of a simple model, the Hinesburg thrust merely emplaced low-permeability (low-K) metamorphic rocks on top of high-permeability (high-K) sedimentary rocks along a ductile fault zone (Fig. 16A). Although based on a smaller dataset (n = 5 versus n = 16), the median yield block for Type IIIA wells, which were completed <30 m below the thrust, is significantly higher than either of those for Type I or Type IIIB wells. An increase in yield for a well completed near the fault zone would be expected in the above scenario as the fault zone would be a place where groundwater from the hanging wall would percolate downward to, through any permeable planar structure(s). Alternatively, the increased yields could be due to the development of secondary porosity in footwall carbonates along/near the fault zone.

In inactive ductile fault zones, Caine *et al.* (2010) suggest that fault zone lithologies may have similar permeabilities to their protoliths. Therefore, mylonites of the hanging wall should have a similar permeability to the lesser-strained metamorphic rocks of their protolith above, and the same could be said about the recrystallized and fractured carbonates of the footwall and their protolith below. The net result of this permeability equivalence would be a low-K hanging wall overlying a high-K footwall, with little affect from the fault zone.

Subsurface chemical hydrogeology

The strong Ca-Mg-HCO_3 signature of Type I (footwall) wells is expected given the dominance of dolostone and limestone in the footwall. Groundwater from Type II (hanging wall) wells trends toward a Na+K-Cl signature because of weathering of mica and albite feldspar (e.g., Reimann & de Caritat 1998) in the metasedimentary rock aquifer of the hanging wall. The fact that some Type II hanging wall wells also have a significant Ca-Mg-HCO_3 component (Fig. 11) likely indicates dissolution of calcite-bearing veins and/or thin marble layers in metamorphosed hanging wall clastic rocks, both of which were observed in the Fairfield Pond and Pinnacle formations during field work by North (2005), Kim *et al.* (2007), Gale *et al.* (2012), and Kim *et al.* (2013). The similarity in major element compositions of hanging wall wells (Type II) and thrust wells (Type IIIA and IIIB) is notable because the

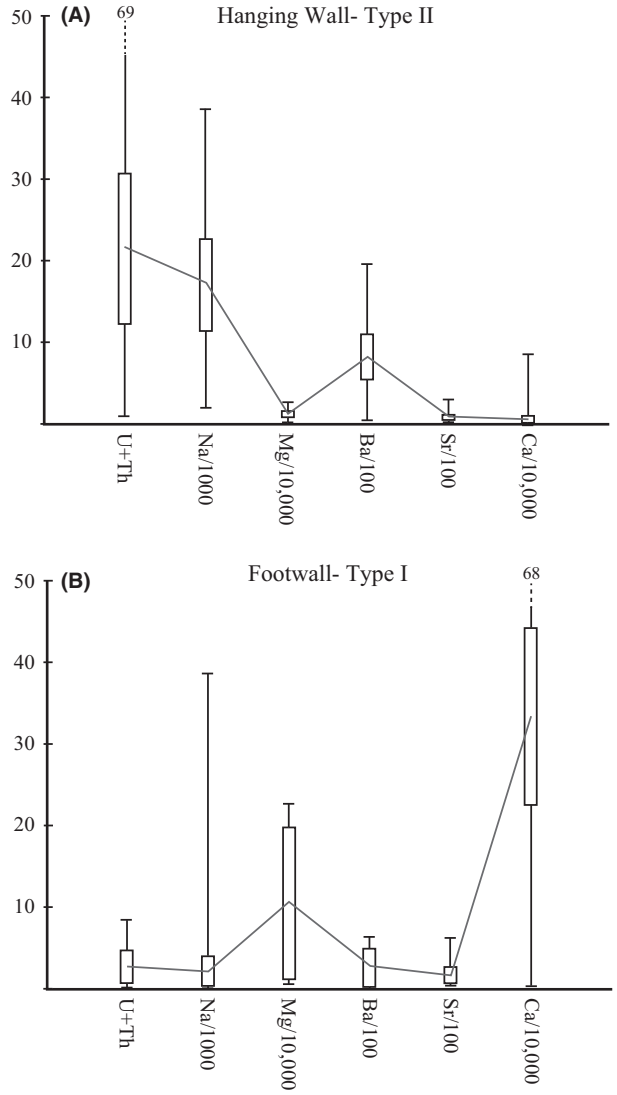

Fig. 15. Box and whisker spider plots showing second and third quartiles (boxes) and minimum and maximum range of data (whiskers) for whole-rock geochemical data from (A) hanging wall and (B) footwall lithologies. In this diagram, U+Th (parts per million) are used as a proxy for gross alpha (picocuries liter^{-1}) and Ca (parts per million) is used as a proxy for alkalinity (parts per million): Na, Mg, Ba, and Sr also in parts per million. See text for explanation.

dominant rock type in the footwall below the thrust is carbonate sedimentary rock. To the west of the thrust front (where there is no hanging wall influence), groundwater is Ca-Mg-HCO_3-rich, so the occurrence of Na+K-Cl groundwater in Type III wells suggests downward flow of hanging wall groundwater through the thrust and into the footwall below the thrust.

Five of six Type III thrust wells display a very similar hydrochemical pattern to groundwater from Type II wells in the hanging wall, with 4 of 6 Type IIIB wells (e.g., 72507-7, KPN102, KPN105, KPN106) showing compositions that are virtually identical to Type II wells (Fig. 14C, D,E and G). Of the two Type IIIA thrust wells sampled, well 80607-2 (Fig. 14B) has a hydrochemical signature that is most similar to Type I footwall groundwater as this well is located closest to the thrust front, suggesting infiltration from the footwall to the west of the thrust exposure; however, the high gross alpha in this well is evidence for some hanging wall influence. Although the higher Na and Sr levels in the other Type IIIA well (KPN101, Fig. 14F) combined with lower Mg and alkalinity levels indicate hanging wall contribution, the lower gross alpha and Ba may reflect some footwall influence. Accordingly, hydrochemical data are consistent with downward flow of groundwater from the hanging wall aquifer to that of the footwall, likely through fractures in the thrust zone (Fig. 7). To integrate the physical and chemical hydrogeology of thrust wells, Type IIIA wells that were completed >30 m below the thrust have a strong hanging wall signature and lower median yields, whereas Type IIIA wells completed closer to the thrust have a more mixed signature and higher median yields.

Box and whisker plots (Fig. 15) that were used to compare rock compositions from hanging wall and footwall show that groundwater chemistry (Fig. 13) with the exception of Sr correlates strongly with rock chemistry. The spider diagrams in Figs 13 and 15 show that rocks and groundwater from the hanging wall have higher median gross alpha, Na, and Ba and lower median Mg and alkalinity, whereas the opposite is true for the footwall. While we have no direct measurements of radioactivity in specific minerals, it is clear that the clastic rocks of the hanging wall are enriched in U and Th as well as Zr, Y, La, and Ce relative to footwall carbonates (Table 5; Table S6). To put the aqueous U data in context, the highest U level in a hanging wall well is 143 ppb, whereas dissolved U in groundwater from U deposits is 70× greater (10 000 ppb) (Jerden & Sinha 2003). There are three probable lithologic sources of radionuclides such as alpha particles, U, Th, and Ra in the hanging wall which are:

1. The hydrolysis of feldspars (e.g., Walley El-Dine *et al.*, 2011) in the Pinnacle, Fairfield Pond, and Cheshire formations. Some metamorphosed quartzite/graywacke lithologies in the Pinnacle formation are classified as arkoses (Cherichetti *et al.* 1998) so detrital feldspars are common. Dissolved Ba is also likely related to dissolution of feldspar (Cecile *et al.*, 1984).
2. Trace minerals such as zircon, apatite, and monazite (e.g., Speer *et al.*, 1981; Reimann and de Caritat, 1998) in clastic hanging wall rocks relative to footwall carbonates. For example, thin section photomicrographs of phyllitic quartzites in the Cheshire formation indicate that U-Th-bearing minerals such as zircon are found along D_3 (=S_3) disjunctive cleavage planes (Fig. 17). Iron oxides and hydroxides are present along D_3 (=S_3)

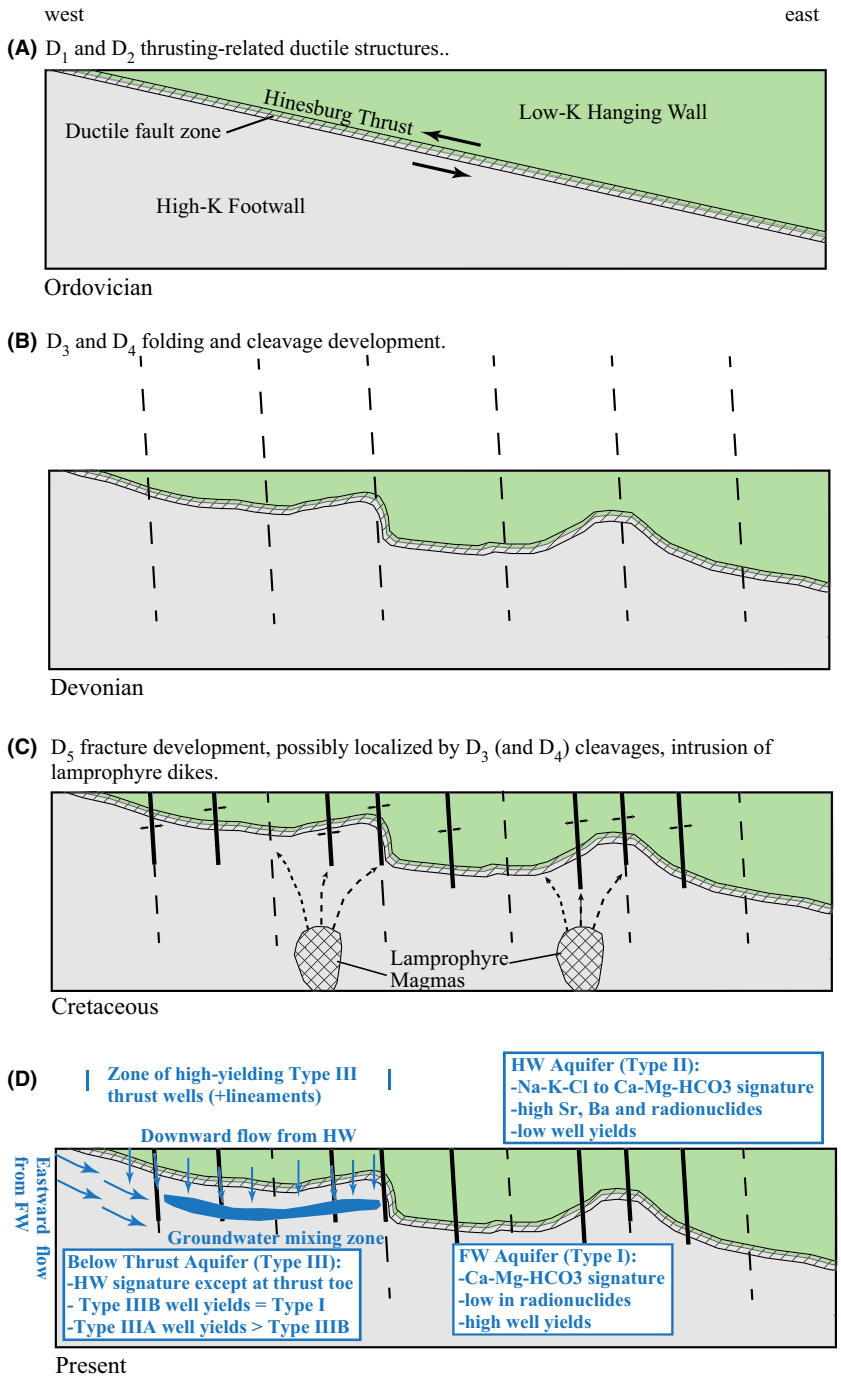

Fig. 16. Time series diagram showing the tectonic evolution of the Hinesburg thrust for the Ordovician (A), Devonian (B), Cretaceous (C), and present (D). A hydrogeological summary is also part of D.

and D_1 ($=S_1$) cleavages, indicating that *in situ* weathering and oxidation occurred along these surfaces. These zircons may either have a metamorphic origin or alternatively, be detrital zircons that were fortuitously enveloped by this cleavage. Although trace minerals such as zircon are very resistant to breakdown in groundwater (Balan *et al.* 2001), internal radiation damage (metamictization) (Woodhead *et al.* 1991) and grain size reduction and dissolution in shear zones (Dempster *et al.* 2008) make zircon and other radionuclide-bearing minerals more susceptible to release of U, Th, and their decay products in groundwater.

3. Alpha recoil has been attributed to release of alpha particles and Ra into solution where parent radionuclide-bearing minerals, such as iron oxyhydroxides, occur along fracture surfaces in bedrock aquifers (Vinson *et al.* 2009; Speer *et al.*, 1981). Also, given that iron oxides and hydroxides are capable of sorbing U (Scott *et al.*

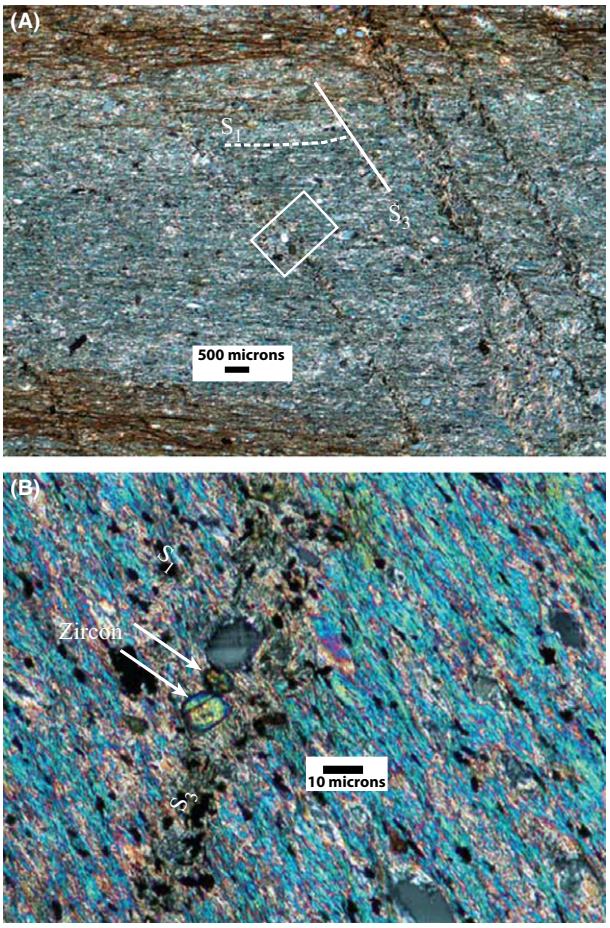

Fig. 17. Photomicrographs of a phyllitic quartzite sample from the Cheshire formation in the hanging wall of the Hinesburg thrust. (A) D_3 disjunctive cleavage superposed on the dominant D_1 foliation (plane polarized light); the D_2 foliation is absent in this part of the field area. Note the brownish coloration caused by iron oxides and hydroxides parallel to S_1 (=D_1) in the upper and lower quarters of this photomicrograph and in S_3 (=D_3) in the right half of this photomicrograph. (B) An enlargement of the inset box on A, which shows zircon grains along a D_3 cleavage plane (crossed polars).

2005), the iron oxides and hydroxides occurring along the fracture planes may also be a source of U.

Once released from the host mineral, U solubility is enhanced by abundant bicarbonate (Langmuir 1997) in both the footwall and hanging wall aquifers.

High Sr values in groundwater from Type II (hanging wall) and Type III (thrust) wells are likely related to Sr concentration in source minerals. Although bulk-rock Sr is lower in hanging wall rocks than footwall rocks (Table 5; Table S6), hanging wall Sr may be enriched by calcite veins and/or thin marble layers in hanging wall metamorphic rocks.

During diagenesis, Sr is released from calcite and dolomite during recrystallization, resulting in low Sr values in diagenetically altered carbonate rocks (typically <100 ppm; Banner 1995) (mean Sr for carbonate rocks in this study is 160 ppm). The Sr that is released from calcite and dolomite migrates into pore waters and is later incorporated into vein calcite, reaching concentrations ranging from 2000 to 40 000 ppm Sr (Powell 1965). Elburg and Bons (2005) found that calcite veins in carbonaceous shales were always enriched in Sr relative to the calcite in the shale host. Based on these studies, we suggest it is possible that the dissolution of calcite veins in the hanging wall could produce groundwater with high Sr relative to footwall groundwater. The migration of hanging wall groundwater across D_5 fractures through the thrust would also result in Type III groundwater with a similar Sr signal to Type II groundwater.

Spatial analysis of geologic and hydrogeologic parameters

The two cross-sections in Fig. 8 demonstrate some important limitations on yields for wells drilled through the Hinesburg thrust. Cross-section A-A′ shows that high well yields are found from the western limit of the thrust to the first large amplitude D_3 fold to the east. Cross-section B-B′ shows the same general trend. This high yield zone also coincides with the area of strongest topographic lineament development in Fig. 5 (also see Fig. 1). The highest yields for Type III wells on the western side of both cross-sections (89–378 lpm) can be due to eastward flow beneath the thrust from the productive footwall aquifer or from westward (and downward) flow from the hanging wall aquifer (Fig. 9), or both. The fact that well 80607-2 (Fig. 14A) is located right at the thrust front has a high yield (189 lpm), and footwall-dominant groundwater geochemistry supports the former. Other thrust wells that were tested in this study have lower yields (11–30 lpm) and, no matter how far they were completed below the thrust surface, have hanging wall-dominated groundwater geochemical signatures. The higher median yields for Type IIIA wells that were completed <30 m below the thrust could imply that the thrust zone is an area where groundwater mixes after leaking downward through the low-K hanging wall.

Moving eastward past the first D_3 fold on cross-section A-A′, the thickness of the hanging wall increases to >400 m and yields decrease to the 0–8 lpm range, even when a second D_3 fold is encountered. As the Hinesburg thrust deepens, the lithostatic load likely closes down any planar structures in the footwall and lower hanging wall that could transmit groundwater.

Figure 12 shows the distribution of radionuclide levels in groundwater throughout the field area. Looking at gross alpha alone, the highest levels in hanging wall (Type II) and thrust (Type III) wells generally occur in/around the Lake Iroquois valley and at/near the western edge of the Hinesburg thrust. The same can be said about U and

RGA/TGA levels. Based on groundwater and surface water flow directions on Fig. 9, both of these areas could be characterized as discharge zones whereas the neighboring highlands are recharge zones. Ryan *et al.* (2013) found that the highest As levels in groundwater from a fractured metasedimentary rock aquifer in southwestern Vermont occurred in low lying discharge zones where groundwater flow paths and residence times in the bedrock aquifer had been the longest. We believe that this study may also apply to our elevated radionuclide occurrences in the hanging wall aquifer and in the footwall aquifer below the Hinesburg thrust, after downward infiltration of groundwater with a hanging wall geochemical signature.

An integrated model

Figure 16 shows a time series for the structural and hydrogeological development of the Hinesburg thrust. The ductile juxtaposition of low-K metamorphic rocks of the hanging wall of the Hinesburg thrust with high-K sedimentary rocks of the footwall created the basic architecture that would later influence the hydrogeology of the field area (Fig. 16A). Although the mylonites that formed on the hanging wall side of this ductile fault zone could be considered a barrier to groundwater flow, it is more likely, however, that their permeability is no different than that of the metamorphic protolith (Caine *et al.* 2010), after fault motion had ceased. The poor exposure of these mylonites precludes a direct evaluation of their permeability structure. D_3 and D_4 folding events (Fig. 16B) deformed the Hinesburg thrust into domes and basins and introduced orthogonal cleavage sets, which probably localized the formation of some D_5 fracture sets and subsequent lamprophyre intrusions (Fig. 16C). As springs flow along some D_5 fracture sets that cut through the mylonites to the fault plane, it is reasonable to assume that these fractures enhanced the hydraulic connection between the hanging wall and footwall aquifers.

Figure 16D summarizes the present day hydrogeology of the Hinesburg thrust using a model of a low-K hanging wall overlying a high-K footwall that has been significantly modified by the development of permeable fracture sets that transect the fault zone. The following points support this model:

1. The median yields of wells completed in the footwall (Type I) far exceed those of the hanging wall (Type II).
2. The median yields of Type IIIA wells (completed <30 m from the thrust) exceed those of Type IIIB wells (completed >30 m from the thrust). This is consistent with the mixing of groundwater that would be expected to occur at/near the interface between the hanging wall and footwall, whether this reflects the permeability contrast between the low-K and high-K rock types alone, the enhanced hydraulic connection across the fault zone provided by fractures, or both. Type IIIB wells have median yields similar to those of Type I footwall wells.
3. The geochemistry of groundwater from most wells completed through Hinesburg thrust (Types IIIA and IIIB) has a strong hanging wall signature. Thrust wells completed near the toe of the thrust may have a footwall or mixed geochemical signature, reflecting the eastward flow of groundwater from the footwall aquifer. The analysis of static water levels in the hanging wall versus footwall indicates a downward gradient, which supports hanging wall-dominant geochemical signatures in thrust wells.

Although many authors (Evans & Chester 1995; Caine & Forster 1999; Fairly & Hinds 2004; Minor & Hudson 2006) note that fault zones exhibit considerable structural and hydrogeological variability along strike, we noticed some consistencies for the Hinesburg thrust. The high yield zone associated with wells drilled through the Hinesburg thrust only persists from the thrust front eastward to the first large amplitude D_3 fold (Fig. 16D); this is possibly due to the fact that the rapid increase in thrust depth (and hanging wall thickness) and corresponding lithostatic pressure after this point closes down structures capable of transporting groundwater. This zone roughly correlates with that of well-developed D_3 topographic lineaments. In addition, the great thrust depths (>500 m) make the thrust more difficult for drill rigs to reach. Along strike thrust wells, with the exception of one well at the thrust front, have a hanging wall geochemical signature.

Appalachian Analogs

In detailed bedrock hydrogeological studies in the Blue Ridge province of Virginia, Seaton & Burbey (2000, 2005) found strongly fractured, highly permeable, and transmissive zones in the brittle crystalline metamorphic rocks above thrust faults. These high-yielding zones were not continuous, but were compartmentalized by local structural and metamorphic factors such as the distribution of quartz veins, which later fractured and provided groundwater breach zones that influenced the volume of recharge. Subordinate faults and lineaments provide conduits for recharge to the confined thrust aquifers. The structural settings of Hinesburg thrust and the Seaton & Burbey (2005) study are generally similar, where a hanging wall of Precambrian crystalline metamorphic rocks of the Blue Ridge was juxtaposed with a footwall comprised of Paleozoic sedimentary rocks of the foreland along a ductile fault zone. However, a fundamental difference is that the Blue Ridge study focused on thrust faults internal to the thick (>1200 m) stack of crystalline slices that tectonically overlie the sedimentary rocks, which were not accessible because of their depth. At present, we do not have evidence for highly fractured and transmissive zones above

thrust faults that are internal to the hanging wall of the Hinesburg thrust. To make the scales of the two studies equivalent, we would also have to include the metamorphic rocks of the hanging wall of the Lake Iroquois Thrust (Figs 1 and 8) on the eastern side of the field area in our study.

CONCLUSIONS

The Hinesburg thrust underwent a protracted and multistage tectonic evolution in which it formed at depth as a ductile fault (D_1 mylonites and associated folding) and moved a second time after 'locking up' (D_2 asymmetric shear bands) during the Ordovician. It was then deformed twice (D_3 and D_4) during the Devonian Acadian orogeny by orthogonal map-scale folds with axial planar disjunctive and crenulation cleavages, and lastly was extensively fractured (D_5) and intruded by lamprophyre magmas during the Cretaceous. Some D_5 fracture sets (approximately north–south and approximately east–west striking) were likely localized by the previously existing D_3 and D_4 cleavages.

From well yield analysis, it is clear that the hanging wall aquifer (Type II wells) is not productive and the footwall aquifer is (Type I wells). We divided wells completed below the Hinesburg thrust into categories depending on whether they were completed <30 m below (Type IIIA) and >30 m below (Type IIIB). Type IIIA wells have the highest median yields of all wells, and Type IIIB wells have median yields in the same range as Type I wells.

The groundwater geochemical signature of the hanging wall and footwall aquifers, with the exception of Sr, correlates strongly with the whole-rock geochemistry of the lithologies in each. The hanging wall aquifer is relatively enriched in alpha radiation (and, uranium), Na+K-Cl, Ba, and Sr, whereas the footwall aquifer is enriched in Ca-Mg-HCO_3 and alkalinity. Both Type IIIA and IIIB wells that penetrated the Hinesburg thrust and were completed in the footwall generally have geochemical signatures trending toward hanging wall compositions, reflecting downward infiltration. However, one Type IIIA well near the thrust front has a footwall-dominated groundwater geochemical signature.

A relatively simple model to integrate the hydrogeology and structural geology of the Hinesburg thrust was constructed, which involves the emplacement of low-K metamorphic rocks of the hanging wall onto high-K sedimentary rocks of the footwall. The fault zone interface of mylonites on the hanging wall side and recrystallized and imbricated carbonates on the footwall side probably have the same permeabilities as their respective protoliths. This structural framework allows for the strong contrast in well yields and the downward infiltration of hanging wall-derived groundwater that mixes in a zone just below the Hinesburg thrust. The downward permeability of the hanging wall and thrust zone was likely enhanced by D_5 fracture development, which may have been localized by previous episodes of cleavage development.

EPILOG: PUBLIC HEALTH APPLICATIONS

During the winter of 2007, the Vermont Geological Survey (VGS) and collaborators from Middlebury College presented a progress report to the Select Board from the Town of Hinesburg. This report included maps and emphasized that elevated radionuclide levels were much more common in bedrock wells completed in the hanging wall than in the footwall. During the spring of 2008, the VGS summarized the results of recent bedrock and surficial mapping and geochemical well testing to the Planning Commission for the Town of Williston. The Vermont Department of Health was frequently advised of elevated radionuclide tests and their geologic context through oral presentations. Based on this work and recommendations by the Vermont Department of Health, many well drillers in Vermont now regularly advise their clients to test for radionuclides. Future testing of groundwater for radionuclides is planned in 2014 south of the current field area in the Bristol and South Mountain quadrangles, where the bedrock framework is nearly identical.

ACKNOWLEDGEMENTS

The authors would like to thank Mark Person (Editor), Chloe Bonamici, and an anonymous reviewer for insightful and comprehensive reviews. We are also grateful to Jonathan Caine and Victor Bense for informal reviews of a preliminary version. In addition, we acknowledge the Vermont Department of Environmental Conservation Laboratory in Waterbury for analyzing the water samples for metals and anions; the Vermont Department of Health Laboratory in Burlington for the Gross Alpha and Radium analyses; the residents of Hinesburg, Williston, and St. George who participated in the groundwater geochemistry portion of this study; and funding from NSF-MRI-R^2-0959306, the Vermont Geological Society and the Middlebury College Student Research Fund, and the Hawley/Mudge funds in the Department of Geology at the University of Vermont.

REFERENCES

Armstrong RL, Stump E (1971) Additional K-Ar dates, White Mountain magma series, New England. *American Journal of Science*, **270**, 331–3.

Balan E, Trocellier P, Jupille J, Fritsch E, Muller J, Calas G (2001) Surface chemistry of weathered zircons. *Chemical Geology*, **181**, 13–22.

Banner JL (1995) Application of the trace element and isotope geochemistry of strontium to studies of carbonate diagenesis. *Sedimentology*, **42**, 805–24.
Bazilchuk N (2000) Tainted water persists. Burlington Free Press, p. 1B. June 5, 2000.
Bean JR (2009) A geochemical analysis of geologic controls on naturally-occurring radioactivity in groundwater, Hinesburg, Vermont. Middlebury College Geology Department, Senior Thesis, p. 66.
Bense VF, Person MA (2006) Faults as conduit-barrier systems to fluid flow in siliciclastic sedimentary aquifers. *Water Resources Research*, **42**, W0542, doi:10.1029/2005WR004480.
Bense VF, Gleeson T, Loveless SE, Bour O, Scibeck J (2013) Fault zone hydrogeology. *Earth-Science Reviews*, **127**, 171–92.
Bruhn RL, Parry WT, Yonkee WA, Thompson T (1994) Fracturing and hydrothermal alteration in normal fault zones. *Pure and Applied Geophysics*, **142**, 609–44.
Cady WM (1945) Stratigraphy and structure of west-central Vermont. *Geological Society of America Bulletin*, **56**, 515–87.
Caine JS, Forster CB (1999) Fault zone architecture and fluid flow: Insights from field data and numerical modeling. In: *Faults and Subsurface Fluid Flow in the Shallow Crust, Geophysical Monograph*, (eds Haneberg WC, Mozley PS, Moore JC, Goodwin LB), pp. 101–27. American Geophysical Union.
Caine JS, Evans JP, Forster CB (1996) Fault zone architecture and permeability structure. *Geology*, **24**, 1025–8.
Caine JS, Ridley J, Wessel ZR (2010) To reactivate or not to reactivate—Nature and varied behavior of structural inheritance in the Proterozoic basement of the eastern Colorado Mineral Belt over 1.7 billion years of earth history. In: *Through the Generations: Geologic and Anthropogenic Field Excursions in the Rocky Mountains from Modern to Ancient*, Vol. **18** (eds Morgan LA, Quane SL), pp. 119–40. Geological Society of America Field Guide 18. doi: 10.1130/2010.0018(06).
Cecile MP, Goodfellow WD, Jones LD, Krouse HR, Shakur MA (1984) Origin of radioactive barite sinter, Flybye springs, Northwest Territories, Canada. *Canadian Journal of Earth Sciences*, **21**, 383–95.
Cherichetti L, Doolan B, Mehrtens C (1998) The Pinnacle formation: a late Precambrian rift valley fill with implications for Iapetus rift basin evolution. *Northeastern Geology and Environmental Sciences*, **20**, 175–85.
Chester FM, Logan JM (1986) Implications for mechanical properties of brittle faults from observations of the Punchbowl fault zone, California. *Pure and Applied Geophysics*, **124**, 79–106.
Cloutier V, Lefebvre R, Savard M, Bourque E, Therrien R (2006) Hydrogeochemistry and groundwater origin of the Basses-Laurentides sedimentary rock aquifer system, St. Lawrence Lowlands, Québec, Canada. *Hydrogeology Journal*, **14**, 573–90.
Coish RA, Sinton CW (1992) Geochemistry of mafic dikes in the Adirondack mountains: implications for late Proterozoic continental rifting. *Contributions to Mineralogy and Petrology*, **110**, 500–14.
Davis L (2008) A geochemical analysis of groundwater and bedrock in Williston, Vermont: An Assessment of Potential Sources of Elevated Radionuclides in Groundwater, Middlebury College Geology Department Independent Study Project, p. 23.
Dempster TJ, Martin JC, Shipton ZK (2008) Zircon dissolution in a ductile shear zone, Monte Rosa granite gneiss, northern Italy. *Mineralogical Magazine*, **72**, 971–86.
Derman K, Kim J, Klepeis K (2008) Three dimensional modeling of an ancient thrust fault surface in the Town of Williston, Northwestern Vermont. Geological Society of America Abstracts with Programs, Vol. **40**, #2, p. 22.
DeSimone LA, Barbaro JR (2012) Yield of bedrock wells in the Nashoba terrane, central and eastern Massachusetts. U.S. Geological Survey Scientific Investigations Report 2012–5155, p. 74. (Also available at http://pubs.usgs.gov/sir/2012/5155).
DiPietro J (1983) Geology of the Starksboro area Vermont, Vermont Geological Survey Special Bulletin No. 4, p. 14, 2 plates, scale 1:24 000.
Donath F (1961) Experimental study of shear failure in anisotropic rocks. *Geological Society of America Bulletin*, **72**, 985–90.
Dorsey RL, Agnew PC, Carter CM, Rosencrantz EJ, Stanley RS (1983) *Bedrock Geology of the Milton Quadrangle, Northwestern Vermont*. Vermont Geological Survey Special Bulletin No. 3, Montpelier, Vermont, p. 14, 4 plates.
Earle H, Kim J, Klepeis K (2010) Comparison of Ductile Structures across the Hinesburg and Champlain Thrust Faults in NW Vermont. Geological Society of America Abstracts with Programs, Vol. **42**, p. 88.
Elburg MA, Bons PD (2005) The origin of fibrous calcite Veins: Aragonite?. EOS, Transactions of the American Geophysical Union, *Fall Meeting Supplement*, **86**, T53C–1451.
EPA (2000) http://www.epa.gov/safewater/radionuclides/pdfs/guide_radionuclides_stateimplementation.pdf
Evans JP, Chester FM (1995) Fluid-rock interaction in faults of the San Andres system: Inferences from San Gabriel fault rock geochemistry and microstructures. *Journal of Geophysical Research*, **100**, 13007–20.
Fairly JP, Hinds JJ (2004) Rapid transport pathways for geothermal fluids in an active Great Basin fault zone. *Geology*, **32**, 825–8.
Filoon JL (2012) A hydrologic, structural, and cartographic analysis of groundwater in the vicinity of the Hinesburg Thrust, west-central Vermont. Middlebury College, unpublished BA thesis, p. 71.
Fisher D (1968) Geology of the Plattsburgh and Rouses Point, New York-Vermont, Quadrangles. Vermont Geological Survey Special Bulletin No. 1, scale- 1:62 500.
Gale MH, Kim JJ, Ruksnis A (2012) Bedrock Geologic Map of the Essex Junction Quadrangle, Vermont: Vermont Geological Survey Open File Map, scale 1:24 000.
Gillespie R (1975) Structure and Stratigraphy along the Hinesburg Thrust, Hinesburg, Vermont. Master's Thesis, University of Vermont Department of Geology, p. 63.
Gudmundsson A (2011) *Rock Fractures in Geologic Processes*. Cambridge University Press, pp. 578.
Gunderson LC (1991) Radon in Sheared Metamorphic and Igneous Rocks. In: *Field Studies of Radon in Rocks, Soils, and Water*, (eds Gunderson LC, Wanty RB), pp. 39–49. U.S. Geological Survey Bulletin 197.
Jerden JL, Sinha AK (2003) Phosphate based immobilization of uranium in an oxidizing bedrock aquifer. *Applied Geochemistry*, **18**, 823–43.
Kim J, Becker L (2001) Geologic context of elevated radionuclide occurrences in NW Vermont. Geological Society of America Abstracts with Programs, Vol. **33**, #1, p. A60.
Kim J, Becker L (2004) Elevated naturally-occurring radioactivity in ground water from 3 fractured bedrock settings in Vermont, National Groundwater Association, Fractured Bedrock Conference, Portland, Maine, Abstracts with Programs, p. 269.
Kim J, Gale M, Thompson P, Derman K (2007) Bedrock Geologic Map of the Town of Williston, Vermont, scale 1:24 000, 3 plates.
Kim J, Klepeis K, Ryan P, Gale M, McNiff C, Ruksznis A, Webber J (2011) A Bedrock Transect Across the Champlain and

Hinesburg Thrusts in West-Central Vermont: Integration of Tectonics with Hydrogeology and Groundwater Chemistry. In: (eds West D), New England Intercollegiate Geological Conference: Guidebook for Field Trips in Vermont and adjacent New York, 103rd Annual Meeting, Middlebury, Vermont. Trip B1, pp. B1-1–-35.

Kim JJ, Weber E, Klepeis K (2013) Bedrock Geologic Map of the Bristol Quadrangle: Vermont. Geological Survey Open File Report, scale 1:24 000, 2 plates.

Kumarpelli PS, Dunning G, Pintson H, Shaver J (1989) Geochemistry and U-Pb Zircon Age of Comenditic Metafelsites of the Tibbit Hill Formation, Quebec Appalachians. *Canadian Journal of Earth Sciences*, **26**, 1374–83.

Landing E, Westrop S, Van Aller Hernick L (2003) Uppermost Cambrian-lower Ordovician faunas and Laurentian platform sequence stratigraphy, eastern New York and Vermont. *Journal of Paleontology*, **77**, 78–98.

Landing E, Amati L, Franzi D (2009) Epeirogenic transgression near a triple junction: the oldest (latest early-middle Cambrian) marine onlap of cratonic New York and Quebec. *Geological Magazine*, **146**, 552–66.

Langmuir D (1997) *Aqueous Environmental Geochemistry*. Massachusetts Department of Environmental Protection, Prentice-Hall, pp. 600. (www.mass.gov/dep/water/drinking/wellyld.pdf)

McHone JG (1978) Distributions, orientations, and ages of mafic dikes in central New England. *Geological Society of America Bulletin*, **89**, 1645–55.

McHone JG (1987) Cretaceous intrusions and rift features in the Champlain Valley of Vermont. In: Guidebook for Field Trips in Vermont, Volume 2: New England Intercollegiate Geological Conference (ed. Westerman D), pp. 237–53.

McHone JG, Corneille ES (1980) Alkalic dikes of the Lake Champlain Valley. *Vermont Geology*, **1**, 16–21.

Mehrtens C (1997) Digital compilation bedrock geologic map of the Lake Champlain South one-degree sheet, Vermont: VGS Open-File Report VG97-01A, 2 plates, scale 1:1 00 000.

Mehrtens CJ, Borre MA (1989) Stratigraphy and bedrock geology of parts of the Colchester and Georgia Plains quadrangles, northwestern Vermont: Vermont Geological Survey Special Bulletin No. 11, p. 29, scale 1:24 000.

Mehrtens CJ, Dorsey R (1987) Stratigraphy and bedrock geology of the northwest portion of the St. Albans and adjacent Highgate Center quadrangles, Vermont: Vermont Geological Survey Special Bulletin No. 9, p. 28, scale 1:24 000.

Mehrtens CJ, Hadley ACH (1995) Stratigraphy and bedrock geology of parts of the St. Albans and Georgia 7.5 minute quadrangles, northwestern Vermont: Vermont Geological Survey Special Bulletin No. 14, p. 18, scale 1:24 000.

Minor SA, Hudson MR (2006) Regional survey of structural properties and cementation patterns of fault zones in the northern part of the Albuquerque Basin, New Mexico: Implications for ground-water flow: U.S. Geological Survey Professional Paper 1719, p. 34.

North K (2005) Evaluation of Geologic Controls on Elevated Naturally-Occurring Radioactivity in Bedrock Groundwater Wells, NW Vermont: Middlebury College, Senior Thesis, p. 77.

Passchier CW, Trouw RA (2005) *Microtectonics*. Springer- Verlag, Berlin, p. 366.

Piper AM (1944) A graphic procedure in the geochemical interpretation of water- analyses: American Geophysical Union Papers, Hydrology, pp. 914–23.

Powell JL (1965) Isotopic composition of strontium in four carbonate vein-dikes. *American Mineralogist*, **50**, 1921–8.

Ramsey JG (1967) *Folding and Fracturing of Rocks*. McGraw-Hill, New York, p. 568.

Reimann C, de Caritat P (1998) *Chemical Elements in the Environment*. Springer, Berlin, p. 398.

Ryan PC, Kim JJ, Mango H, Hattori K, Thompson A (2013) Arsenic in a fractured slate aquifer system, New England, USA: influence of bedrock geochemistry, groundwater flow paths, redox and ion exchange. *Applied Geochemistry*. http://dx.doi.org/10.1016/j.apgeochem.2013.09.010

Salvini F, Billi A, Wise DU (1999) Strike-slip fault-propagation cleavage in carbonate rocks: the Mattinata fault zone, Southern Apennines, Italy. *Journal of Structural Geology*, **21**, 1731–49.

Scott TB, Allen GC, Heard PJ, Lewis AC, Lee DF (2005) The extraction of uranium from groundwaters on iron surfaces. *Proceedings of the Royal Society A*, **461**, 1247–59.

Seaton W, Burbey T (2000) Aquifer characterization in the Blue Ridge physiographic province using resistivity profiling and borehole geophysics: geologic Analysis. *Journal of Environmental and Engineering Geophysics*, **5**, 45–58.

Seaton W, Burbey T (2005) Influence of Ancient Thrust Faults on the Hydrogeology of the Blue Ridge Province. *Groundwater*, **43**, 301–13.

Speer JA, Solberg TN, amd Becker SW (1981) Petrography of the uranium-bearing minerals of the Liberty Hill Pluton, South Carolina: phase assemblages and migration of uranium in granitoid rocks. *Economic Geology*, **76**, 2162–75.

Springston GE (2008) Terrain analysis using Lidar topographic data: a case history from Williston, northwest Vermont (abs.): Geological Society of America, Northeastern Section Meeting Abstracts with programs, no. 2, Vol. **40**, p. 66.

van Staal CR, Dewey JF, Niocaill CM, McKerrow WS (1998) The Cambrian- Silurian tectonic evolution of the northern Appalachians and British Caledonides: history of a complex, west and southwest Pacific-type segment of Iapetus. In: *Lyell: the Past is the Key to the Present*, Vol. **143** (eds Blundell DJ, Scott AC), pp. 199–242. Geological Society, London, Special Publications.

Stanley RS, Ratcliffe NM (1985) Tectonic synthesis of the Taconian orogeny in western New England. *Geological Society of America Bulletin*, **96**, 1227–50.

Stanley R, Wright S (1997) The Appalachian foreland as seen in northern Vermont. In: Guidebook to field trips in Vermont and adjacent New Hampshire and New York: New England Intercollegiate Geological Conference, Vol. **89** (eds Grover TW, Mango HN, Hasenohr EJ), pp. B1–33.

Stanley R, Dellorusso V, O'Loughlin S, Lapp E, Armstrong T, Prewitt J, Kraus J, Walsh G (1987) A Transect through the Pre-Silurian Rocks of Central Vermont. In: Guidebook for Field Trips in Vermont, New England Intercollegiate Geological Conference (ed. Westerman D), pp. 272–95.

Strehle B, Stanley R (1986) A comparison of fault zone fabrics in Northwestern Vermont [4 sites in Milton, Mechanicsville (Hinesburg), South Lincoln (Lincoln), and Jerusalem (Starksboro)], p. 36, 4 plates.

Tauvers P (1982) Bedrock geologic map of the Lincoln area, Vermont, Vermont Geological Survey Special Bulletin No. 2, p. 8, 1 plate, scale 1:24 000.

Thompson T, Thompson P, Doolan B (2004) Bedrock Geologic Map of the Hinesburg Quadrangle, Vermont Geological Survey Open File Map VG04-2, scale- 1:24 000.

Twiss RJ, Moores EM (2007) *Structural Geology*. W.H. Freeman and Co., New York, p. 736.

Vermont Department of Health Online Fact Sheets. Gross alpha radiation- http://healthvermont.gov/enviro/rad/alpha.aspx,

Uranium- http://healthvermont.gov/enviro/rad/Uranium.aspx.
Vinson DS, Vengosh A, Hirschfeld D, Dwyer GS (2009) Relationships between radium and radon occurrence and hydrochemistry in fresh groundwater from fractured crystalline rocks, North Carolina (USA). *Chemical Geology*, **260**, 159–71.
Walley El-Dine N, El-Shershaby A, Afifi S, Sroor A, Samir E (2011) Natural radioactivity and Rare Earth elements in feldspar samples, Central Eastern desert, Egypt. *Applied Radiation and Isotopes*, **69**, 803–7.
Walsh G, Aleinikoff J (1999) U-Pb Zircon Age of Metafelsite from the Pinney Hollow Formation: implications for the Development of the Vermont Appalachians. *American Journal of Science*, **299**, 157–70.
Welby CW (1961) Bedrock geology of the central Champlain Valley of Vermont. Vermont Geological Survey Bulletin, v. **14**.
Whitehead M (2008) The petrographic and geochemical analysis of lamprophyre dikes in Williston, Vermont, Middlebury College, Senior Thesis, p. 82.
Woodhead JA, Rossman GR, Silver LT (1991) The Metamictization of Zircon: radiation Dose-Dependent Structural Characteristics. *American Mineralogist*, **76**, 74–82.

SUPPORTING INFORMATION

Additional Supporting Information may be found in the online version of this article:

Table S1 Well-log data.

Table S2 Water sampling details.

Table S3 Analytical methods and precision for groundwater geochemistry.

Table S4 Analytical methods and precision for whole-rock geochemistry.

Table S5 Complete groundwater geochemical dataset.

Table S6 Complete whole-rock geochemical dataset.

GEOFLUIDS

Volume 14, Number 3, August 2014
ISSN 1468-8115

CONTENTS

WILEY
Blackwell

Geofluids* is abstracted/indexed in *Chemical Abstracts

This journal is available online at Wiley Online Library.
Visit onlinelibrary.wiley.com to search the articles and register for table of contents and e-mail alerts.